1967

Experimental Analysis of Free Convection Heat Transfer From a Nonisothermal Plate

Lloyd Edwin Stoebner

EXPERIMENTAL ANALYSIS OF FREE CONVECTION HEAT TRANSFER FROM A NONISOTHERMAL PLATE

BY

LLOYD EDWIN STOEBNER

A thesis submitted
in partial fulfillment of the requirements for the
degree Master of Science, Major in
Mechanical Engineering, South
Dakota State University

1967

EXPERIMENTAL ANALYSIS OF FREE
CONVECTION HEAT TRANSFER FROM
A NONISOTHERMAL PLATE

This thesis is approved as a creditable and independent investigation by a candidate for the degree, Master of Science, and is acceptable as meeting the thesis requirements for this degree, but without implying that the conclusions reached by the candidate are necessarily the conclusions of the major department.

Thesis Adviser Date

Head, Mechanical Engineering Department Date

ACKNOWLEDGMENTS

It seems fitting that the author should recognize the assistance and counseling of Professor B. E. Eno who aided greatly in the analytical considerations, the assistance of Mr. R. E. Lundin who helped in the fabrication of the test model and stand, and to others who assisted in various ways.

LES

TABLE OF CONTENTS

LIST OF FIGURES

LIST OF TABLES

NOMENCLATURE

A - area of plate (width times thickness, shown in Figure 3)

A_s - exposed surface area of plate

b - plate width in z-direction

c_p - specific heat at constant pressure

g - acceleration due to gravity

Gr - Grashof number $\left[g \beta (T_w - T_\infty) x^3 \right] / \nu^2$

h_x - local heat transfer coefficient defined by Equation (3-9)

I - amperes

K_A - thermal conductivity of air

K_M - thermal conductivity of plate

L - length of plate

n - refractive index of air

ΔN - fringe-shift

Pr - Prandtl number (ν/α)

q - heat transfer rate

Q - total heat transfer

q''' - internal heat generation

T_w - temperature of wall

T_∞ - temperature of ambient fluid

u - velocity component in x-direction

v - velocity component in y-direction

V - volts

x - coordinate measuring distance along plate from bottom leading edge

y - coordinate measuring distance normal to plate

z - coordinate measuring width of plate

α - thermal diffusivity $(k_f/\rho c_p)$

β - coefficient of thermal expansion

δ - momentum boundary layer thickness

δ_t - thermal boundary layer thickness

ϵ - radiation emissivity

λ - wave length of laser beam

ν - kinematic viscosity

ρ - fluid density

σ - Stefan-Boltzmann's constant

ψ - stream function

CHAPTER I

INTRODUCTION

Heat transfer by convection has been studied extensively since about 1900, but it is probably still the least understood of the three types of heat transfer due to its dependency on fluid dynamics. The most thoroughly studied cases are forced convection over a flat plate and free convection from a vertical isothermal plate. In a large number of engineering applications, it is necessary to calculate the heat transfer from a surface which is heated locally such as a fin heated at its root. There has been very little analytical or experimental work done for this particular case in which the internal conduction within the plate is coupled with the convection away from the plate.

The purpose of this investigation is to study the free convection heat transfer from a thin vertical flat plate of uniform thickness which is heated locally at various vertical positions. The laws which govern the heat transfer phenomenon are reviewed as they relate to the problem. Due to the complexity of the resulting equations, it will be necessary to rely on experimentation to determine the heat transfer characteristics. The total heat transfer and heat transfer coefficient will be calculated from the experimental data and the results will be compared to a more idealized case consisting of an isothermally heated plate.

The report will first present the governing laws as they apply to the problem. An explanation of the experimental analysis will be next, followed by a discussion of the results. Finally, rather brief conclusions and recommendations will be given.

CHAPTER II

REVIEW OF RELATED LITERATURE

The idealized case of free convection from a vertical flat plate has been solved by the approximate von Karman integral technique. This solution may be found in many elementary texts such as Holman [1] .* To effect this solution, it is necessary to assume velocity and temperature profiles within the boundary layer. The results obtained by this approximate technique compare favorably with the exact solution and experimental verification of Pohlhausen, Schmidt, and Beckmann as related by Eckert and Drake [2].

Sparrow and Gregg [3] present an exact solution for uniform heat-flux rate at the surface of a vertical flat plate. The continuity, momentum, and energy partial differential equations were transformed into ordinary differential equations by applying a variable transformation. These equations were solved numerically for Prandtl numbers of 0.1, 1.0, 10, and 100. The theoretical results compare very closely to the experimental results obtained by Dotson [4].

Using the von Karman integral technique, Sparrow [5] assumed polynomials for velocity and temperature profiles and solved the problem of free convection from a vertical plate having either a specified non-uniform surface heat-flux or temperature distribution

---

*Bracketed numbers refer to references listed in the bibliography.

along the plate. Approximate solutions for the total heat transfer and heat transfer coefficient were found and compared to a more idealized case of an isothermally heated plate.

Sparrow and Gregg [6] also carried out a theoretical analysis for laminar free convection from a vertical plate with the surface temperature distributions given as

$$T_w - T_\infty = Nx^n \qquad \text{and} \qquad T_w - T_\infty = Me^{mx}$$

where N, n, M, and m are constants. Exact solutions for the total heat transfer and local heat transfer coefficient were calculated using a similarity transformation. Numerical solutions were calculated for Prandtl numbers of .7 and 1.0.

CHAPTER III

MATHEMATICAL ANALYSIS

Theoretical Model

The theoretical model which will be used in this analysis is shown in Figure 1 below.

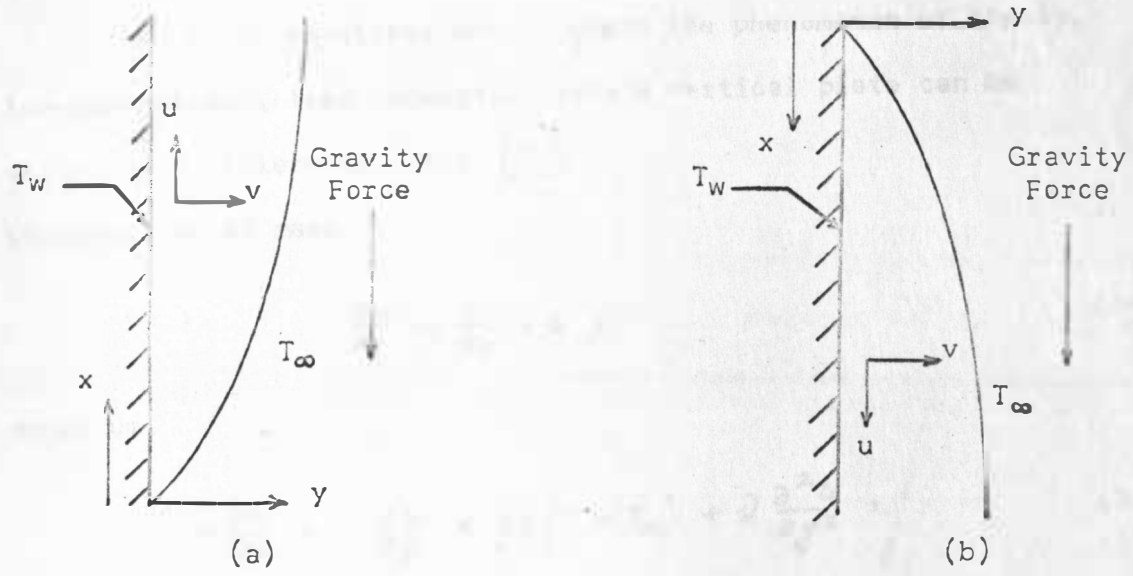

Figure 1

Figure 1(a) depicts the situation to which the local wall temperature T_w exceeds the ambient temperature T_∞, and heat is being transferred from the wall to the fluid. Figure 1(b) represents the situation in which the ambient temperature T_∞ exceeds the wall temperature T_w, and heat is being transferred from the fluid to the wall.

The analysis will be carried out for Figure 1(a) wherein heat is being transferred from the wall to the fluid. It should be noted, however, that if the coordinate system is taken as shown in Figure 1(b), then the analysis and results would be the same for both situations.

Governing Equations

The basic equations which govern the phenomenon of steady, two-dimensional, free convection from a vertical plate can be stated as in Eckert and Gross [7]:

conservation of mass,

$$\frac{\partial u}{\partial x} + \frac{\partial v}{\partial y} = 0 \ , \tag{3-1}$$

momentum,

$$u\frac{\partial u}{\partial x} + v\frac{\partial u}{\partial y} = g\beta\left(T - T_\infty\right) + \nu\frac{\partial^2 u}{\partial y^2} \ , \tag{3-2}$$

and energy,

$$u\frac{\partial T}{\partial x} + v\frac{\partial T}{\partial y} = \alpha\frac{\partial^2 T}{\partial y^2} \ . \tag{3-3}$$

The following assumptions were made during the derivation of these equations:

a) steady state

b) two-dimensional

c) viscous and conduction effects are contained in a thin boundary layer

d) no internal heat generation (q''') within the plate

e) negligible viscous dissipation

f) the fluid properties β, ν, and α in Equations (3-2) and (3-3) will be taken as constants at the film temperature.

In attempting to effect an exact solution from Equations (3-1), (3-2), and (3-3), one could introduce a stream function ψ which would satisfy the continuity equation (3-1). Upon substitution of the stream function into Equations (3-2) and (3-3), the result would be two simultaneous equations in two unknowns, ψ and T. Ordinary differential equations could be obtained if a variable transformation can be introduced. However, before such a transformation can be established, it is necessary to know the temperature distribution along the surface of the plate.

An alternative approach would be to use the von Karman integral technique to develop an approximate solution consisting of integrating Equation (3-2) and (3-3) from y = 0 to y = δ where δ equals the boundary layer thickness. For free convection, the integral momentum equation and the integral energy equation as stated by Holman [1] are respectively:

$$\frac{d}{dx}\left[\int_0^{\delta} \rho u^2 dy\right] = -\mu \left.\frac{\partial u}{\partial y}\right|_{y=0} + \int_0^{\delta_t} g\rho\beta(T-T_\infty)\,dy \qquad (3\text{-}4)$$

and

$$\frac{d}{dx}\left[\int_0^{\delta_t} u(T-T_\infty)dy\right] = -\alpha \left.\frac{\partial T}{\partial y}\right|_{y=0} \qquad (3\text{-}5)$$

The thermal boundary layer thickness is defined as the distance measured from the wall to a point at which $T_w - T = .99 (T_w - T_\infty)$. It is within this laminar boundary layer that longitudinal convection and transverse conduction are predominant.

The hydrodynamic boundary layer thickness may be defined as the distance measured from the wall to a point at which $u = .01\ u_{max}$. It is within this layer that viscous forces are in effect giving rise to a velocity profile in the fluid. Since the bouyancy force caused by the temperature variation in the fluid gives rise to the motion within the boundary layer, the thermal and hydrodynamic boundary layer thicknesses are approximately equal as may be noted in Equations (3-4) and (3-5).

The von Karman integral equations can only be solved by the proper substitution of the velocity and temperature profiles. These profiles are approximated by assuming polynomials in y to a particular order which will satisfy the boundary conditions for the velocity and temperature at the plate and at $y = \delta_t$. One boundary condition, either the temperature or the temperature gradient, must be specified at the plate. A typical pair of profiles for a plate heated to T_w is shown in Figure 2.

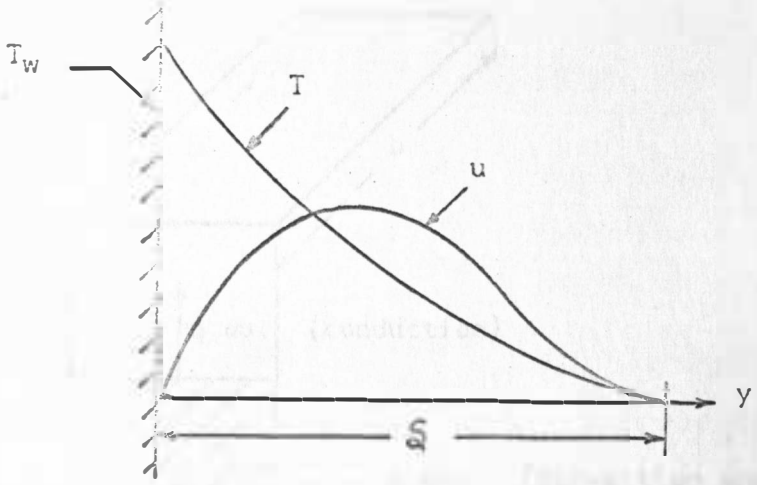

Figure 2

Once these profiles are derived, subsequent integration of the von Karman integral equations will result in first order differential equations in terms of the independent variable x. In order to integrate this, it is necessary to specify either the plate temperature or temperature gradient at every x location up the plate.

In the present problem, not only is there convection and radiation away from the plate, but there is conduction up the plate. Thus, to establish the appropriate heat balance within the plate, it is necessary to consider an infinitesimal element dx of the plate as shown in Figure 3.

The convection away from the plate is governed by Newton's Cooling Law

$$\frac{q}{A} = h\left(T_w - T_\infty\right) \tag{3-7}$$

where h is defined as the convection heat transfer coefficient. The conduction in the fluid at the wall is governed by Fourier's Conduction Law

$$\frac{q}{A} = -K_A \left.\frac{\partial T}{\partial y}\right|_{y=0} \tag{3-8}$$

where $\left.\frac{\partial T}{\partial y}\right|_{y=0}$ is the temperature gradient evaluated at the wall. By coupling Equation (3-7) with (3-8) at the wall, one can solve for the coefficient as

$$h_x = -\frac{K_A \left.\frac{\partial T}{\partial y}\right|_{y=0}}{T_w - T_\infty} \tag{3-9}$$

where h_x is the local heat transfer coefficient.

Using Newton's Cooling Law along with the Stefan-Boltzman's Law for radiation in Equation (3-6) results in

$$-K_m A \frac{dT_w}{dx} = -K_m A \frac{dT_w}{dx} + \frac{d}{dx}\left(-K_m A \frac{dT_w}{dx}\right)dx + \sigma \epsilon b dx \left(T_w^4 - T_\infty^4\right) + h_x b dx \left(T_w - T_\infty\right) \tag{3-11}$$

where the shape factor has been taken as unity. Rearrangement of Equation (3-11) results in

$$\frac{d^2 T_w}{dx^2} - \frac{h_x b}{K_m A}\left(T_w - T_\infty\right) - \frac{\sigma \epsilon b}{K_m A}\left(T_w^4 - T_\infty^4\right) = 0. \tag{3-12}$$

As mentioned previously in outlining the procedure for obtaining the exact solution, the variable transformation in the momentum and energy equation could not be established without a specification of the wall temperature which in the present case is a function of x. In essence, this means that the velocity and temperature profiles cannot be derived until the wall temperature is specified; however, it is readily seen from Equation (3-12), that the wall temperature is governed by an equation which contains the heat transfer coefficient h, and this in turn is governed by Equation (3-9). Therefore, a coupling effect exists between Equations (3-2), (3-3), and (3-12) and these must be solved simultaneously, a virtually impossible task.

The same dilemma exists in attempting the approximate solution. The resulting first order differential equations in x also must have the plate temperature distribution specified. Once again it may be seen that this distribution can only be specified by Equation (3-12); thus, a coupling effect exists again and will not afford a solution.

The experimental program was devised to obtain the plate temperature distribution and to measure the temperature gradient in the fluid adjacent to the plate. Using Equation (3-9), the heat transfer coefficient h_x could be empirically derived and subsequently the local convection heat transfer can be calculated. Total heat transfer results can be obtained by numerical integration.

CHAPTER IV

EXPERIMENTAL EQUIPMENT

Interferometer

A sophisticated instrument which shows the density variations in a two-dimensional flow field is a Mach-Zehnder interferometer. A beam of monochromatic light is split into two identical beams at a partial reflecting mirror. One beam is directed past a heated surface while the other is not. The interference pattern is formed by recombining the beams at another partial reflecting mirror. The distortion of the resulting fringe pattern is indicative of the temperature profile in front of the plate.

Knofczynski [8] built a 6-inch Mach-Zehnder interferometer which is housed in the Mechanical Engineering Research Laboratory at South Dakota State University. The original light source was an AH-4 100 watt GE mercury arc lamp. However, the intensity was not sufficient to produce clear, distinct interferograms, especially for transient convection studies. A neon-helium continuous gas laser was substituted as the light source. A schematic layout of the interferometer with the laser is shown in Figure 4. The laser beam was slightly divergent. This was used to advantage by reflecting the beam off M_1 and M_2 (Figure 4) and passing it through a diverging lens so that a beam radius was obtained which would produce a 6-inch

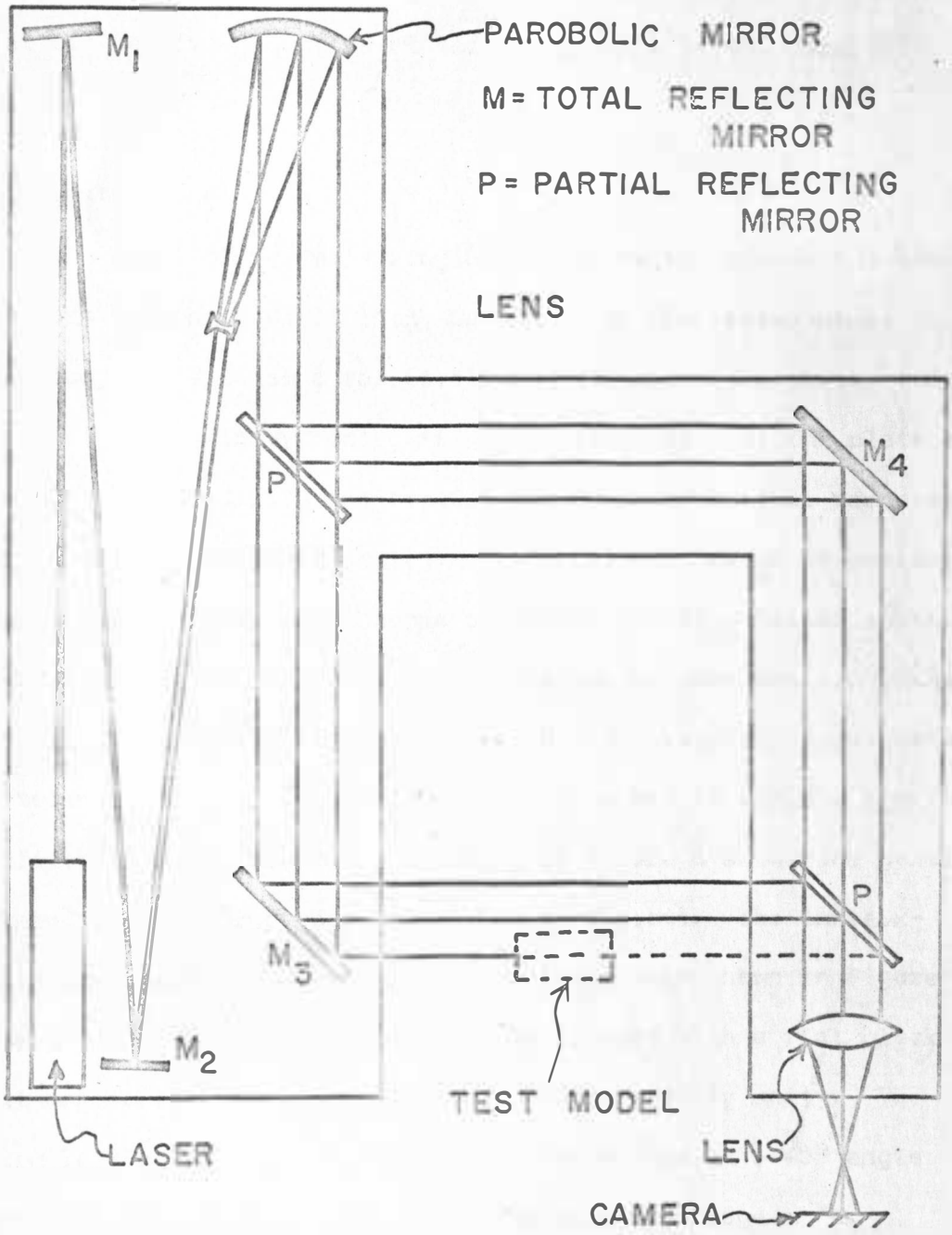

SCHEMATIC OF MACH-ZEHNDER INTERFEROMETER

FIGURE 4

diameter beam on the parabolic mirror. To obtain a collimation after the parabolic mirror, it was necessary to place the focal point of the diverging lens at the focal point of the parabolic mirror.

Experimental Model

A steel plate, measuring 30 inches by 6.5 inches and having a uniform thickness of .1 inch, was used for the heated model in this study. Steel has a relatively low thermal conductivity compared to copper or aluminum; hence, it was possible to heat the plate at a particular x-locality and produce a nonuniform surface temperature distribution in the x-direction. The plate was heated at various x-locations by a 400 watt Chromalox induction strip heater shown by the arrow in Figure 5. Because the heating element was 1.5 inches wide, it was advantageous to place a .5-inch strip of copper between the test plate and the heating element in order to achieve a more localized line of heating. Section A of Figure 6 shows the contact between the heater, copper strip, and test plate. The three x-positions used for the heater placement are also shown in Figure 6. The exposed face of the test plate was sprayed with a flat black paint making the radiation emissivity approximately unity. The bottom leading edge of the test plate was milled at a 45° angle (Section A, Figure 6) to provide a sharp leading edge.

Thirty copper-constantan thermocouples were soldered into the plate for monitoring the plate temperature. The thermocouple wires, size 24 B & S, covered with Fiberglas insulation, were

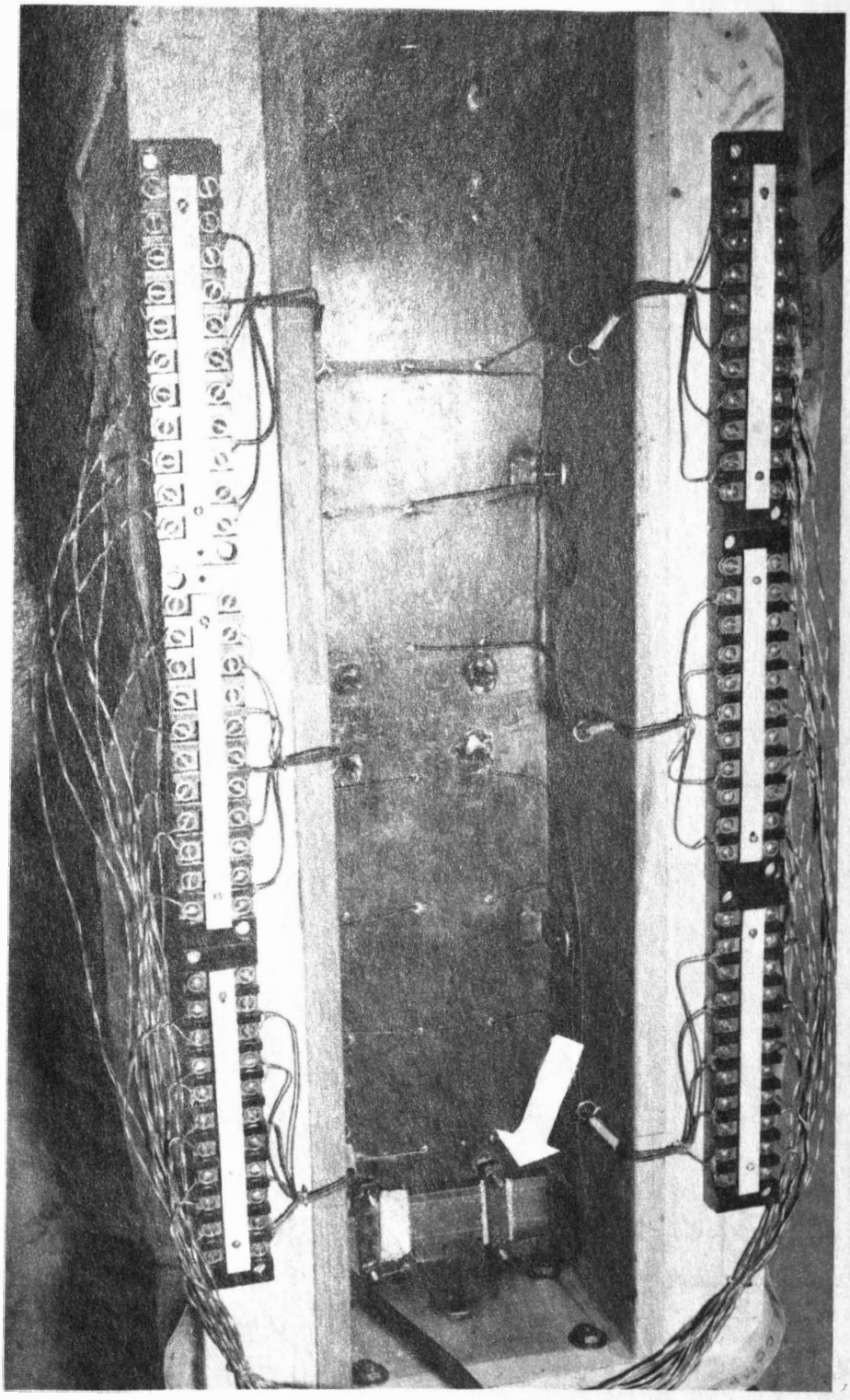

Figure 5. Rear View of Test Model

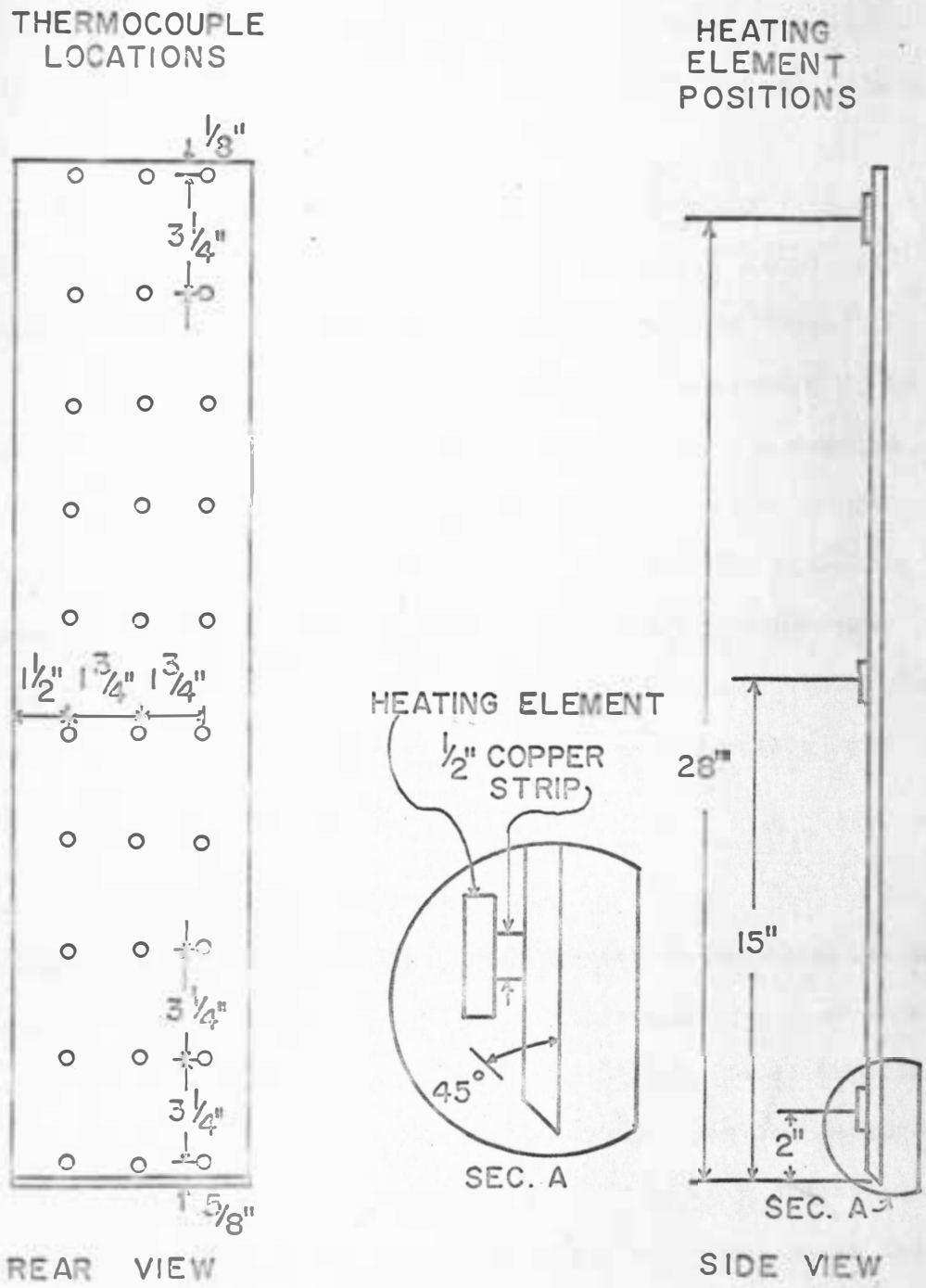

FIGURE 6 SCHEMATIC OF THE TEST PLATE

welded by an electric spark discharge welder to make the proper junctions. The thermocouples were positioned as shown in Figures 5 and 6. Junction boards at the back of the test model were used to contact the thermocouple wires to 12-foot extension wires leading to the switching units.

The test plate was clamped in a redwood shell exposing only one face (Figures 5 and 7). The purpose of this wooden shell was a) to hold the test plate in position, and b) to provide insulation around the edges of the plate and enable Fiberglas insulation to be packed behind the test plate eliminating convection up and conduction out the back of the plate. To insure that the heat loss from the back side and edges of the test plate would be a minimum, a 3-inch thick layer of Fiberglas insulation was placed around the redwood shell. To allow views of the convection process at every x-position along the plate surface, the test model stand was adjustable in a vertical direction as may be seen from Figure 7.

Experimental Procedure and Data Accumulation

The first step in the experimental procedure was to align the test plate paralled to the light beam; the undisturbed fringes were then aligned perpendicular to the plate. The heating power supplied to the plate was controlled by a Variac Autotransformer and measured by an A.C. voltmeter, ammeter and wattmeter. To achieve steady state conditions, the test plate was heated approximately three hours before data was taken.

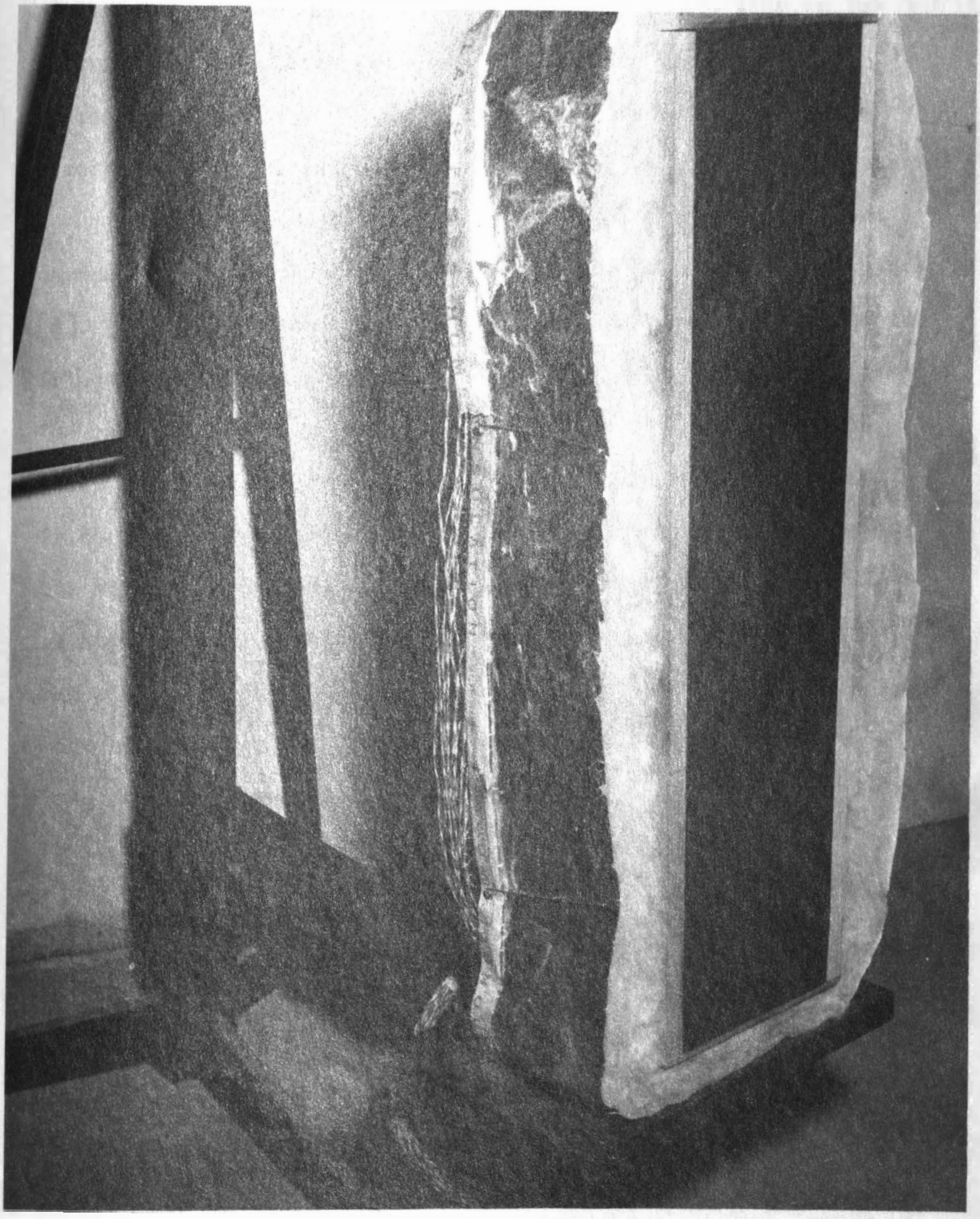

Figure 7. Test Stand and Model

A Leeds and Northrup precision potentiometer with an ice bath reference junction was used to obtain the temperatures of the thermocouples. Room temperature was recorded from a thermometer hung at approximately the same level as the interferometer.

The fringes were photographed using a Graflex 4 x 5 Land camera. The correct placement of the camera is shown by Knofczynski [8]. The bellows were extended to the point where the image of the fringes covered the height of the ground glass in back of the camera. The exposure time was set for one second and the f-stop at 4.5. Kodak Super Panchro-Press type B film was used to photograph the fringes. These photographs were enlarged to either a 5 x 7 or an 8 x 10 print depending upon whether the photograph contained a low or high temperature difference between the plate and room temperature respectively. Since the photographs were enlarged, correct measurement of dimensions in the interferogram analysis was aided by inserting a calipers set at a known dimension into the light path. Photographs taken at various x-positions along the plate were designated by numbers inserted between the calipers as shown in Figures 8 and 9 of Chapter 5.

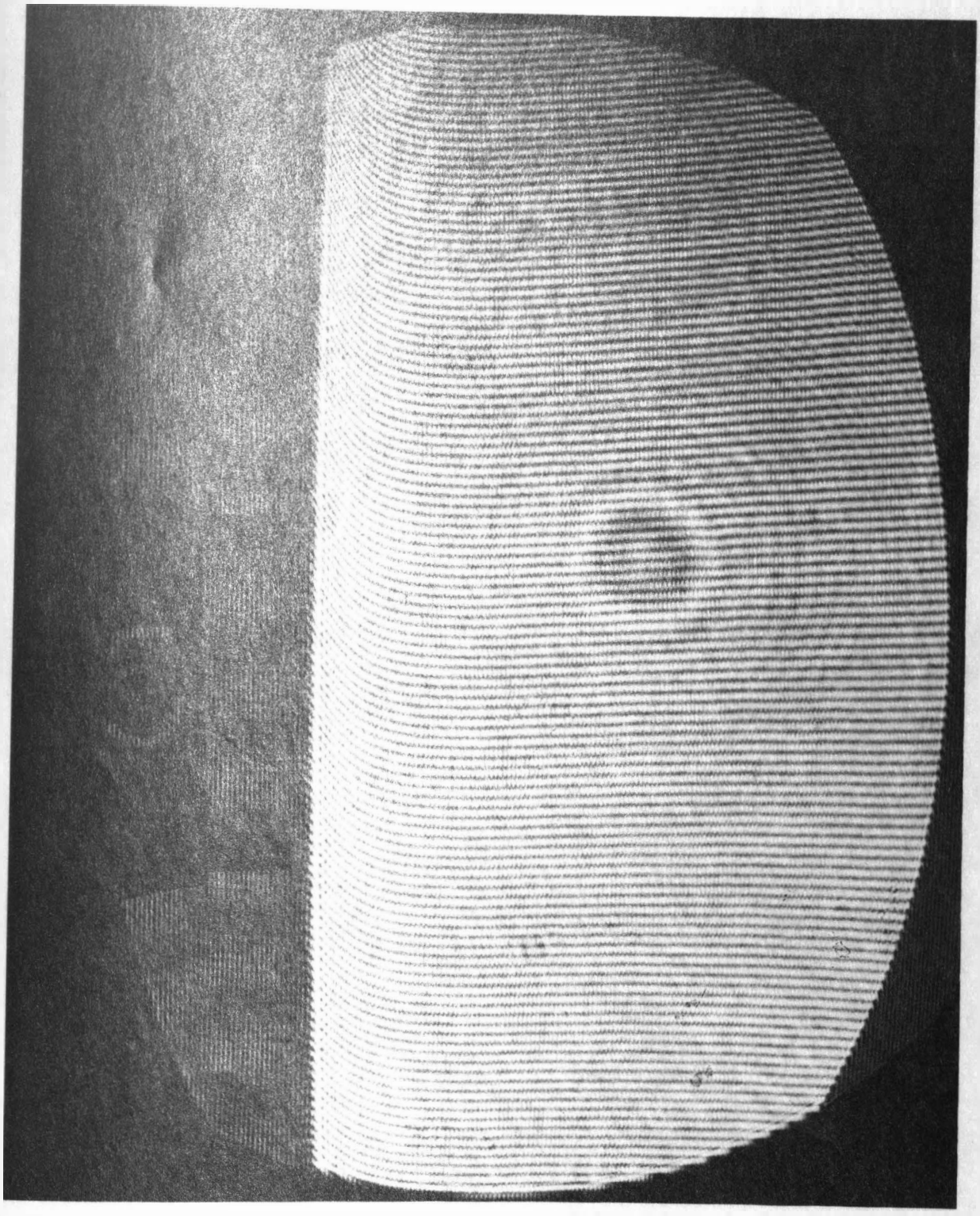

Figure 8. Interferogram for x = 25 inches with Heating Element at x = 28 inches and 100.36 watts

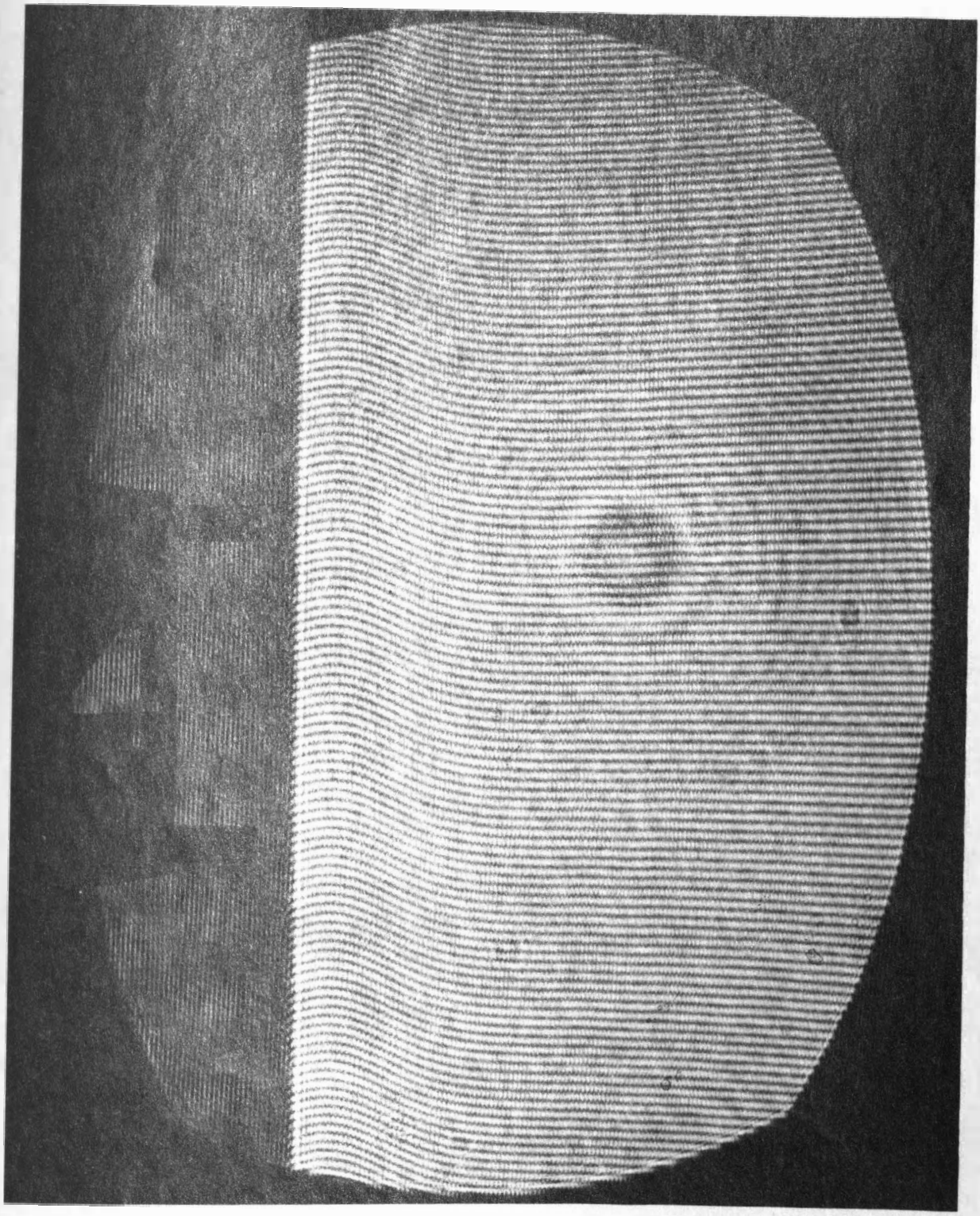

Figure 9. Interferogram for x = 25 inches with Heating Element at x = 2 inches and 79.34 watts

temperatures were recorded from a potentiometer and the results are shown on Figure 10. The curves are in general agreement with the interferograms except very close to the wall. It is felt that the thermocouple, which was unshielded, received radiation heat transfer and thus would not indicate the decreasing temperature in close proximity to the wall.

The method derived by Kennard [9] to calculate the temperature gradient at the wall is in error when the maximum slope does not occur at the wall as is the case in Figure 9. When this occurred in this analysis, an indirect method was used to obtain the gradient. For the case in which the heating element was near the top of the plate (x = 28 inches), the reversed convection phenomenon did not occur because the portion of the plate below the heating element was heated solely by conduction. In this case the value of the gradient at the plate could be calculated and correlated to the slope (θ) of the isothermal fringe at the wall intersection. A graph was then made plotting $\left.\frac{dT}{dy}\right|_{y=0}$ versus θ. For the case in which the reversed convection phenomenon occurred, the temperature gradient could be obtained from the graph by measuring the angle of the fringe at the wall with respect to the undisturbed fringe in the ambient field. It is essential for accurate analysis that the angle be measured with respect to the undisturbed fringe rather than the plate surface because it is possible that the undisturbed fringe is not aligned perpendicular to the plate.

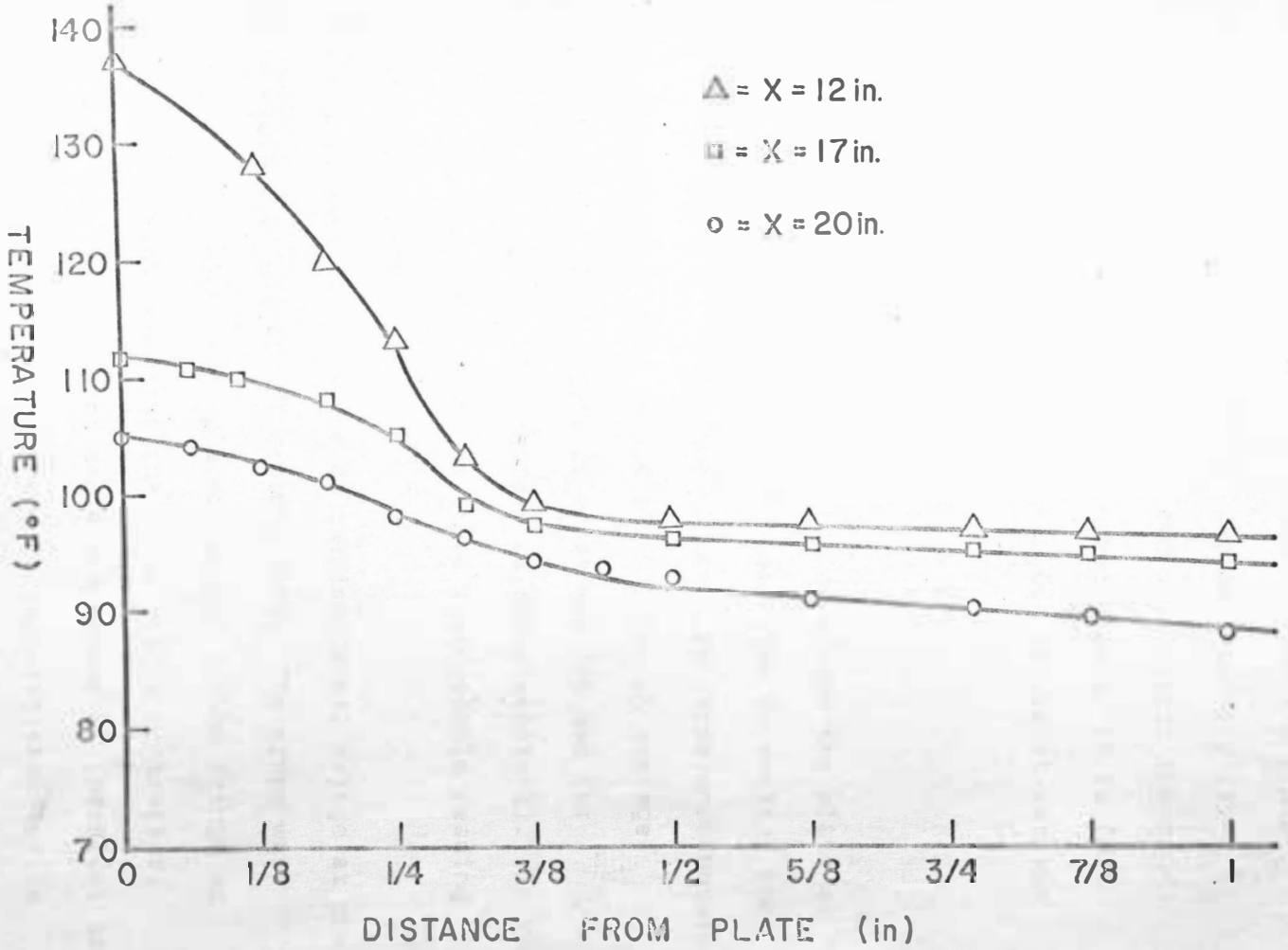

FIGURE 10 TEMPERATURE PROFILE OF AIR IN BOUNDARY LAYER

It should be noted at this point that for the calculation of the gradient, the distance Δy was measured from the plate surface to a point which was .95 of the thermal boundary layer thickness. This is an arbitrary choice and will affect the magnitudes of the local heat transfer, but nevertheless, it is felt that a fair comparison may be made of the local values at various positions up the plate.

Accuracy of Measurement

Three thermocouples in the z-direction across the plate at each of ten vertical positions (Figure 6) were used to monitor the temperature of the plate. The maximum temperature difference between any three horizontal thermocouples was 10.5° F for an average temperature of 284° F. This degree of error was not bad for approximating the free convection pattern as two-dimensional. In the analysis, an arithmetic average of the three thermocouple readings at each x-location was used.

The measurement of the slope of the isothermal fringe at the wall was the least accurate of all measurements. The slope was obtained by using a straight edge placed tangent to the fringe at the wall intersection and measuring the angle with a protractor. The maximum error occurred when the angle approached 0° (parallel to the undisturbed fringe); however, the convection heat transfer is very small if not negligible in this area so the error could be tolerated.

The measurement of the power supplied is considered very accurate because the voltmeter and ammeter used were precision instruments accurate to within $\frac{1}{2}$ % of full scale readings. Since the heating element was a simple resistor with a power factor of unity, the total power was obtained by multiplying voltage times amperage.

End Effects

The equations used for evaluating interferograms for the temperature and temperature gradient are based on a true two-dimensional free convection pattern. Since the present case involves a finite width (6.5 inches), the edges contribute a local three-dimensional effect. Kennard [9], who used a 4-inch wide plate, recommended that a correction factor of 5% of the total plate width be added to this width. Since the plate width in this investigation was 62.5% wider, a smaller correction factor should be incorporated. However, according to Rich [10], the 5% correction factor should be higher for temperatures around 300° F. Since experiments were conducted for temperatures around and above 300° F, it was felt that the two effects would cancel. Therefore, the correction factor used for this investigation was 5% of the total plate width.

CHAPTER VI

DISCUSSION OF RESULTS

Plate Surface Temperatures

The plate temperature distributions as recorded from the thermocouples for the three heating element positions are shown in Figures 11, 12, and 13. Four power settings were used for each heater position with the exception of the position at x = 2 inches. In this case, turbulent flow was observed for the 100 watt power setting. Since the convection phenomenon for turbulent flow is markedly different than laminar flow, the trial was neglected.

As mentioned in the previous chapter, the only heating element position where the temperature and temperature gradient equations using the Kennard fringe-shift method can be utilized is for the position at x = 28 inches. Therefore, this is the only heater position for which the temperature was calculated by the Kennard fringe-shift method. The calculated values are compared with the thermocouple readings for the four power settings and are shown in Table I. With the exception of the 100 watt power setting, it can be observed that the temperatures do not compare very favorably in contrast to the small error achieved by other investigators using interferometry. The maximum error for the 100 watt power setting is 3.35%, which is within experimental error, compared to 8.64%, 7.52%, 5.80% for the 80, 60, and 40 watt power settings respectively. The error is possibly due to either a faulty battery in the potentiometer or because the plate was nonisothermal, therefore, not lending itself

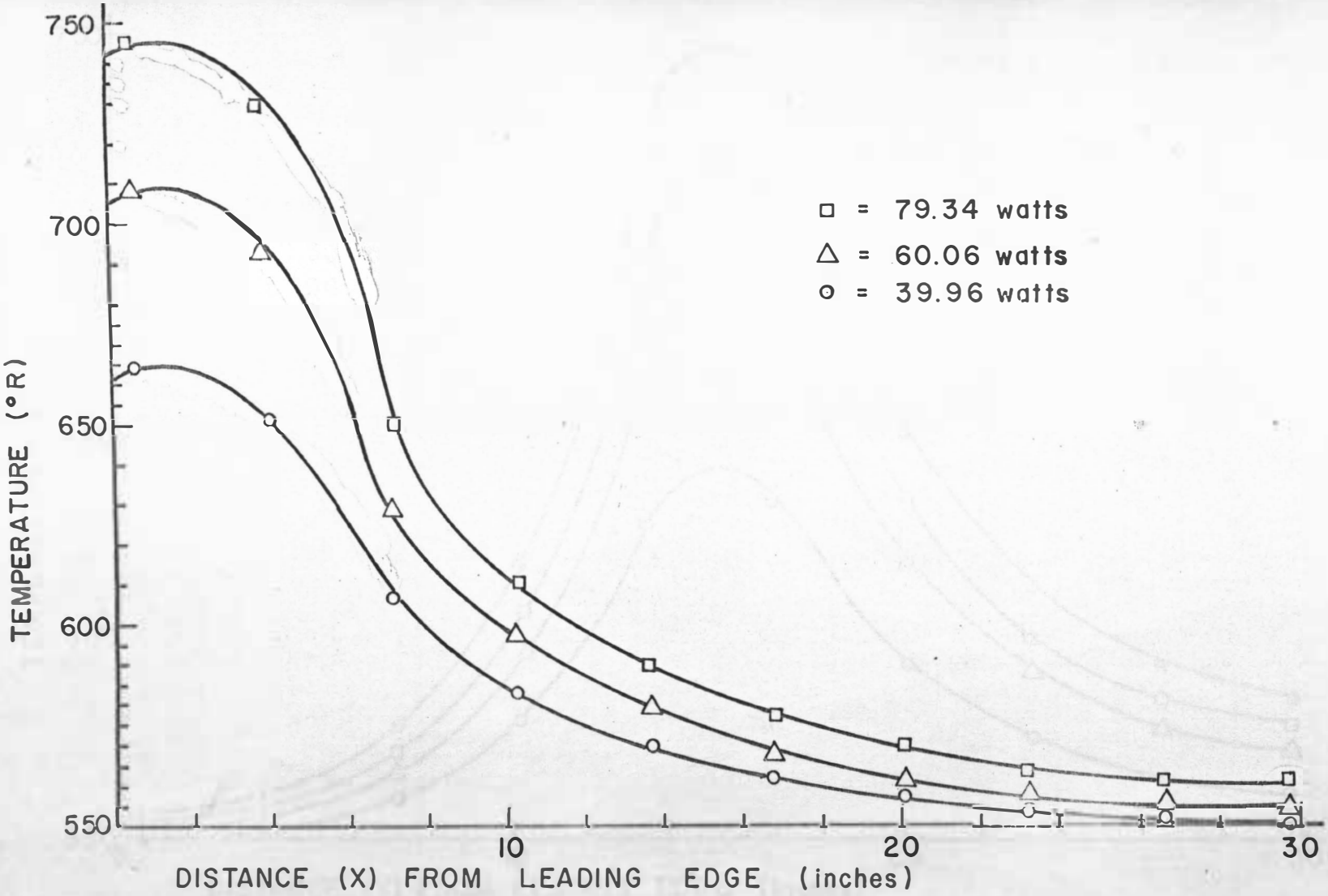

FIGURE 11 TEMPERATURE DISTRIBUTION FOR HEATING ELEMENT AT X=2 INCHES

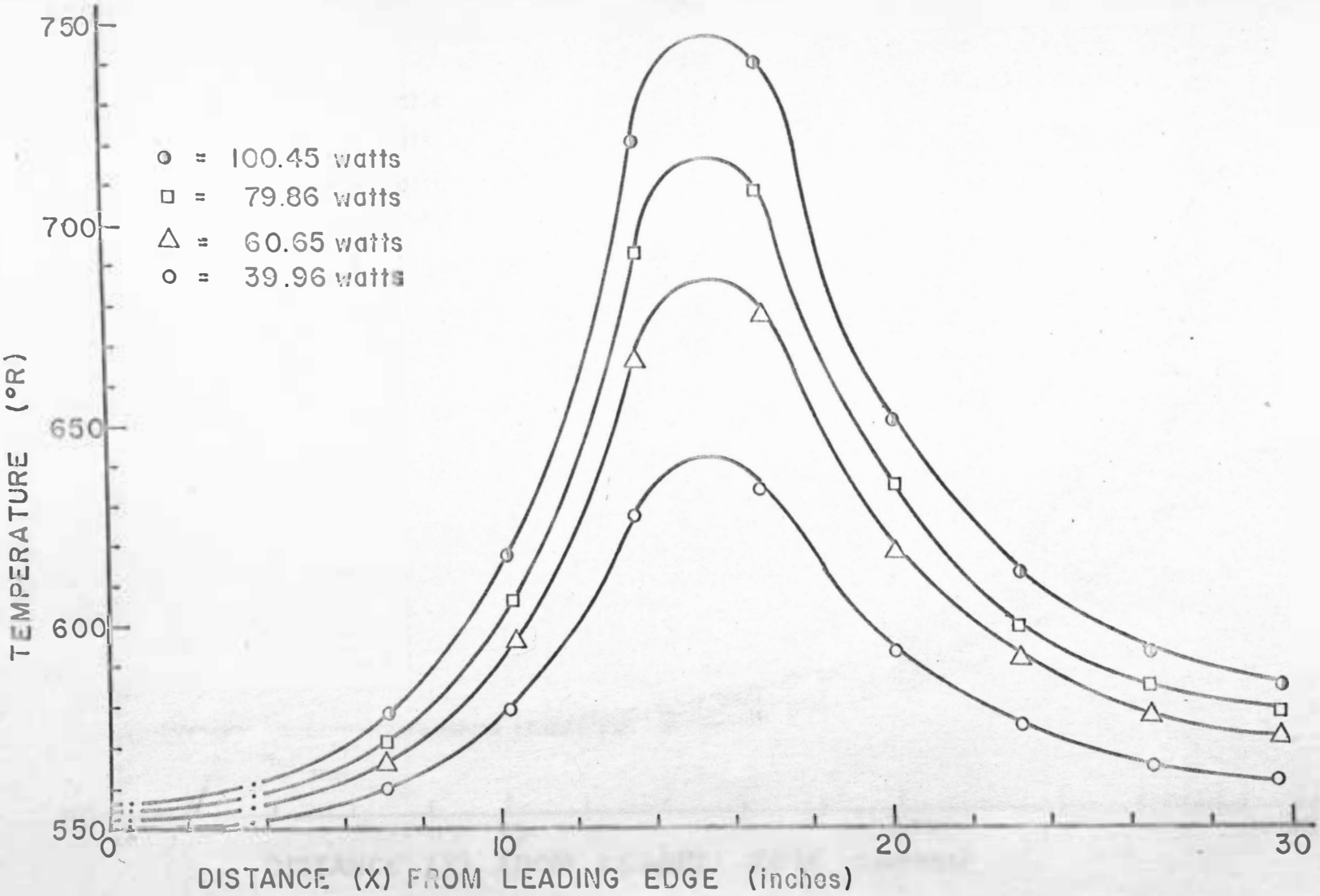

FIGURE 12 TEMPERATURE DISTRIBUTION FOR HEATING ELEMENT AT X = 15 INCHES

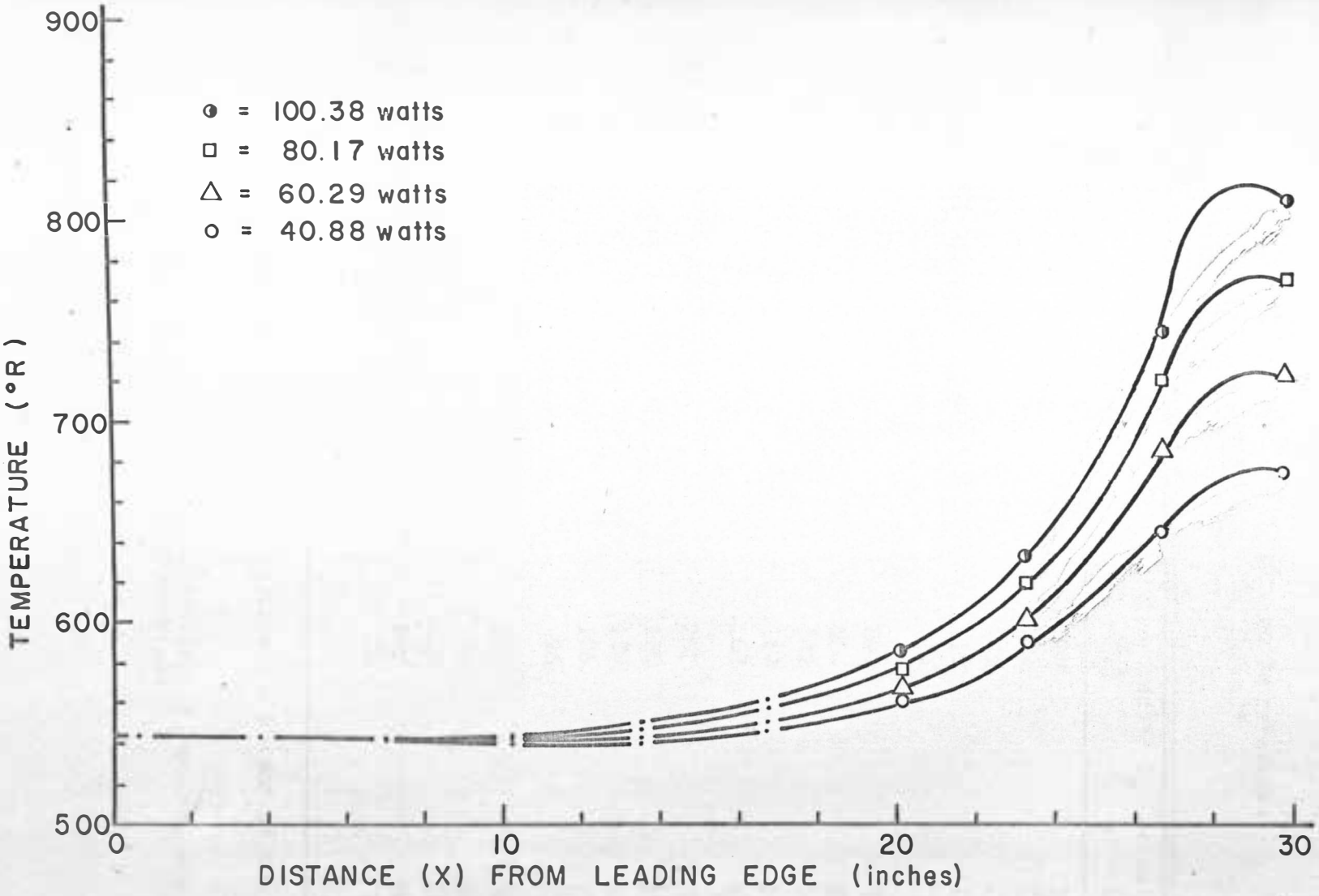

FIGURE 13 TEMPERATURE DISTRIBUTION FOR HEATING ELEMENT AT X=28 INCHES

TABLE I

Comparison of Measured and Calculated Temperatures
(Heating Element at x = 28 inches)*

Power (watts)	x (inches)	T_w (measured)** (^oF)	T_w (calculated) (^oF)
100.38	27.5	330	335
	25.0	224	227
	22.0	149	154
	19.0	118	117
	17.0	104	101
80.17	27.5	290	315
	25.0	204	212
	22.0	142	147
	19.0	117	115
	16.0	102	100
60.29	27.5	251	270
	25.0	180	188
	22.0	130	133
	19.0	106	109
	16.0	96	98
40.88	27.5	208	220
	25.0	163	169
	22.0	120	125
	19.0	103	105
	16.0	94	94

* "x" designates distance measured from the bottom of the plate

** Values recorded were taken from the graphs representing temperature versus distance up the plate

to the Kennard fringe-shift method. Although the battery in the potentiometer was purchased new, it had to be replaced approximately a week after the data was taken for this investigation. Hence, the battery was probably weak during the recording of the data giving random erroneous temperatures, that is, for one trial the error may be positive while the next trial it may be negative.

Comparison of Heat Lost to Heat Supplied

A comparison of the heat lost to heat supplied was made for each trial. The radiation effects were calculated using the Stefan-Boltzmann's Law

$$\frac{q}{A} = \sigma \epsilon \left(T_w^4 - T_\infty^4 \right). \qquad (6\text{-}1)$$

Since the plate was painted a flat black, the emissivity, ϵ, was assumed to be unity. The plate temperature at various vertical positions and the room temperature were known so the radiation heat transfer per unit area could be calculated. The distribution was then numerically integrated and the total radiation heat transfer was obtained.

The convection heat transfer effects were calculated using Fourier's Conduction Law [Equation (3-4)]

$$\frac{q}{A} = -k \left. \frac{\partial T}{\partial y} \right|_{y=0} \qquad (3\text{-}4)$$

The temperature gradient at the wall, $\left. \frac{\partial T}{\partial y} \right|_{y=0}$, was obtained from the interferogram analysis as described in the previous chapter. The resulting convection heat transfer distribution was numerically

integrated to determine the total convection heat transfer from the plate. Heat conduction losses from the back and edges of the plate were neglected because the test model was insulated. The calculated values of the plate heat losses are compared to the power supplied in Table II.

From the table, it can be seen that the error between the heat lost and heat supplied is very significant. One reason for this is the assumption of measuring Δ_j as the distance from the wall to a point .95 of the thermal boundary layer thickness. A certain degree of random error may also exist because of the potentiometer error previously discussed. From Equation (6-1) for the calculation of the radiation effects, it can be seen that the measured wall temperature is raised to the fourth power and any slight error in this temperature would produce an appreciable radiation error. The total heat transferred from the plate would thus be greatly affected because, for a plate with an emissivity of unity, the per-cent of the total heat lost by radiation is approximately 80% as reported by Rich [10].

Convection Heat Transfer Coefficient

The local convection heat transfer coefficient was calculated using Equation (3-9)

$$h_x = -\frac{K_A \left.\frac{\partial T}{\partial y}\right|_{y=0}}{T_{w_x} - T_\infty} \qquad (3\text{-}9)$$

The method of determining these quantities has already been discussed. The coefficient was plotted as a function of x and the results are

TABLE II

Comparison of Heat Lost to Heat Supplied

Heating Element Position x (inches)*	Q_{conv} (Btu/hr)	Q_{rad} (Btu/hr)	Q_{total} (lost) Q (Btu/hr)	(supplied) (Btu/hr)
2	16.2	65.6	81.8	136.0
	32.2	151.0	183.2	204.5
	75.8	256.0	331.8	277.0
15	11.6	44.3	55.9	136.0
	18.6	109.9	128.5	206.0
	36.5	182.0	218.5	276.0
	124.8	285.8	410.6	342.0
28	14.9	32.0	46.9	136.0
	38.4	70.2	108.6	206.0
	70.3	150.0	220.3	276.0
	93.5	234.5	328.0	342.0

* "x" designates the distance from the bottom of the plate

shown as curve C on Figures 14-24 of Appendix A. It should be noted at this time that the negative heat transfer coefficient which appears on some graphs merely indicates that heat is being transferred in the opposite direction, that is, from the air to the plate.

No empirical heat transfer coefficient was derived from the present experimental results because of the limited data accumulated. Without an appropriate correlation applicable to the present case being available, one might attempt to use a more idealized correlation such as that for the free convection from an isothermal plate. It would be interesting to make a comparison between the heat transfer coefficient distribution based upon the present experimentation to those that would be determined using the isothermal plate correlation. This latter correlation, referred to in Chapter 2, is given in Holman [1] as

$$\frac{hx}{k_f} = 0.508\, Pr^{\frac{1}{2}} (0.952 + Pr)^{-\frac{1}{4}} (Gr_x)^{\frac{1}{4}} \qquad (6\text{-}2)$$

In this correlation, the properties k, ρ, and ν were evaluated at the film temperature of air.

Two methods of treatment using Equation (6-2) were devised to account for the wall temperature T_w. The first method consisted of calculating mean temperatures from the measured plate temperature distributions and substituting these values for T_w into Equation (6-2). The results obtained are shown as curve A on the graphs in Appendix A.

The second method consisted of using the actual point-by-point plate temperature measured experimentally at various x-positions as the T_w and calculating the local heat transfer coefficient from Equation (6-2). These are shown as curve B on the graphs in Appendix A.

Total Convection Heat Transfer

The total convection heat transfer from the plate was calculated for each of the two methods using the isothermal correlation and the results are compared to the experimental case in Table III. For the first method (mean temperature), the total heat transfer was calculated using the average heat transfer coefficient found by integration of h_x over the plate length L.

$$\bar{h} = \frac{1}{L}\int_0^L h_x\,dx = \frac{4}{3}\,h_{x=L} \qquad (6\text{-}3)$$

The results from the second method (actual plate temperature from experimental data) were obtained by numerical integration of the heat transfer per unit area over the plate length. Since according to the correlation, the heat transfer coefficient approaches infinity at the leading edge of the plate where the boundary layer thickness is theoretically zero, the heat transferred from the first $\frac{1}{2}$ - inch of the plate was set equal to the heat transferred in the second $\frac{1}{2}$ - inch of the plate (from $x = \frac{1}{2}$ inch to $x = 1$ inch). Although this would introduce a slight error in the total heat transfer from the plate, it is felt that the error is considerably less in this case than to assume that the heat transfer approaches infinity.

TABLE III

Convection Heat Transfer Results

Heater Position x (inches)	Power Setting (watts)	Convection Heat Transfer q_A (Btu/hr)	q_B (Btu/hr)	q_C (Btu/hr)
2	39.96	23.3	50.2	16.2
	60.06	36.2	74.5	32.2
	79.34	52.4	187.1	75.8
15	39.96	19.2	21.9	11.6
	60.65	36.0	40.0	18.6
	79.86	51.6	54.3	36.5
	100.45	63.0	70.4	71.7
28	40.88	16.1	24.8	14.9
	60.29	21.2	44.0	38.4
	80.17	33.4	49.8	70.3
	100.38	42.3	75.8	93.5

x = The distance from the bottom of the plate.

h_A = The convection heat transfer calculated for an isothermal plate having an average temperature.

h_B = The convection heat transfer calculated for an isothermal plate using actual point-by-point temperatures.

h_C = The convection heat transfer from the test plate.

CHAPTER VII

CONCLUSIONS

The main conclusions drawn from this investigation for free convection heat transfer are:

1. For a thin plate, the internal resistance in the vertical direction is sufficiently high such that, when the plate is heated at one x-locality, it is possible that the convective movement adjacent to the surface exceeds the conduction up the plate causing the heat to be transferred back into the plate further up the surface. The convection back into the plate is given up by radiation, thus not resulting in a net heating of the upper part of the plate. It must be noted, however, that the physical explanation was not definitely verified.
2. The local heat transfer coefficient and the total convection heat transfer for a plate having a variable surface temperature cannot be predicted or calculated accurately by the employment of an isothermal correlation.

CHAPTER VIII

RECOMMENDATIONS

The following recommendations are made.

1. The test model built for this investigation may be used for a number of other experiments:
   a) A more extensive study may be undertaken similar to the present investigation for the determination of an empirical relationship showing that the heat transfer coefficient may be a function of the fluid properties, plate material properties, plate dimensions, local heating position, and power supplied.
   b) It may also be used to experimentally study the characteristics of convective turbulent flows either by using an isothermal plate or a variable temperature plate as was used in this investigation.
2. Another test model may be built, similar to the one used, to study the problem of optimum spacing of isothermal or nonisothermal fins.

BIBLIOGRAPHY

1. Holman, J.P., Heat Transfer, McGraw-Hill Book Company, Inc., New York, New York, 1963, pp. 160-162.

2. Eckert, E.R.G. and Drake, R.M. Jr., Heat and Mass Transfer, 2nd ed., McGraw-Hill Book Co., Inc., New York, New York, 1959, p. 315.

3. Sparrow, E.M. and Gregg, J.L., "Laminar Free Convection From a Vertical Plate with Uniform Surface Heat Flux, "Trans. ASME, Vol. 78, 1956, pp. 435-440.

4. Dotson, J.P., "Heat Transfer From a Vertical Plate by Free Convection," M.S. Thesis. Purdue University, W. Lafayette. Ind., May, 1954, as reported by [3].

5. Sparrow, E.M., "Laminar Free Convection on a Vertical Plate with Prescribed Nonuniform Wall Heat Flux or Prescribed Nonuniform Wall Temperature," NACA TN 3508, 1955.

6. Sparrow, E.M. and Gregg, J.L., "Similar Solutions for Free Convection From a Nonisothermal Vertical Plate," Trans. ASME, Vol. 80, 1958, pp. 379-386.

7. Eckert, E.R.G. and Gross, J.F., Introduction to Heat and Mass Transfer, McGraw-Hill Book Co., Inc., New York, New York, 1963, pp. 96-97, 118.

8. Knofczynski, C., "Design and Construction of a 6-Inch Mach-Zehnder Type Interferometer," M.S. Thesis, South Dakota State University, 1965.

9. Kennard, R.B., "An Optical Method for Measuring Temperature Distributions and Convection Heat Transfer," Journal of Research, U.S. National Bureau of Standards, Vol. 8, 1932,

10. Rich, B.R., "An Investigation of Heat Transfer From an Inclined Flat Plate in Free Convection," Trans. ASME, Vol. 75, 1953, pp. 489-499.

APPENDICES

APPENDIX A

HEAT TRANSFER COEFFICIENT DISTRIBUTIONS

Figure 14 - Figure 24

Graph Nomenclature

A = Heat transfer coefficient distribution for the isothermal plate using the mean temperature from the measured plate temperature distribution for T_w.

B = Heat transfer coefficient distribution for the isothermal plate using the actual point-by-point measured plate temperatures for T_w.

C = Heat transfer coefficient distribution for the test plate.

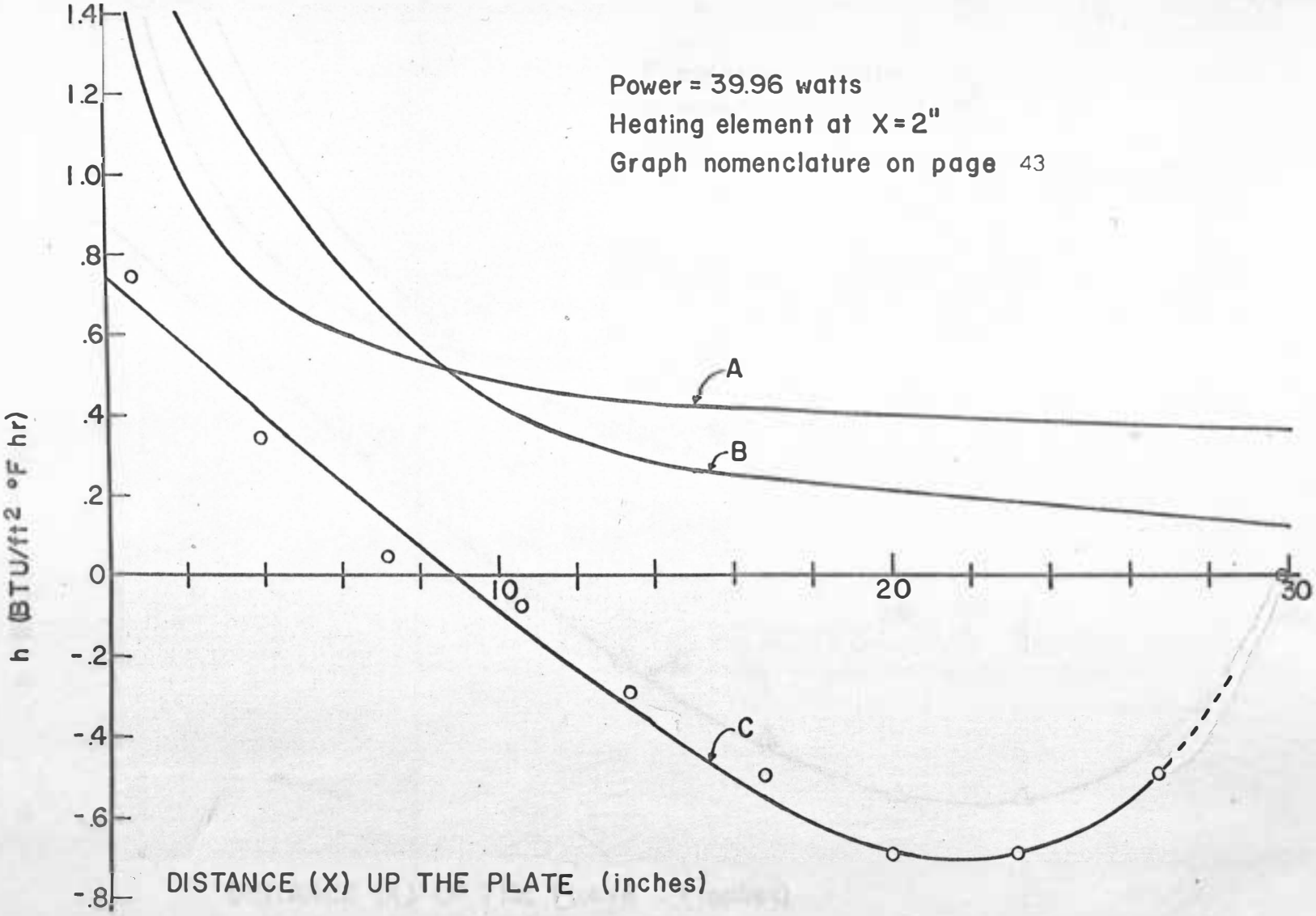

FIGURE 14 DISTRIBUTION OF HEAT TRANSFER COEFFICIENT (h)

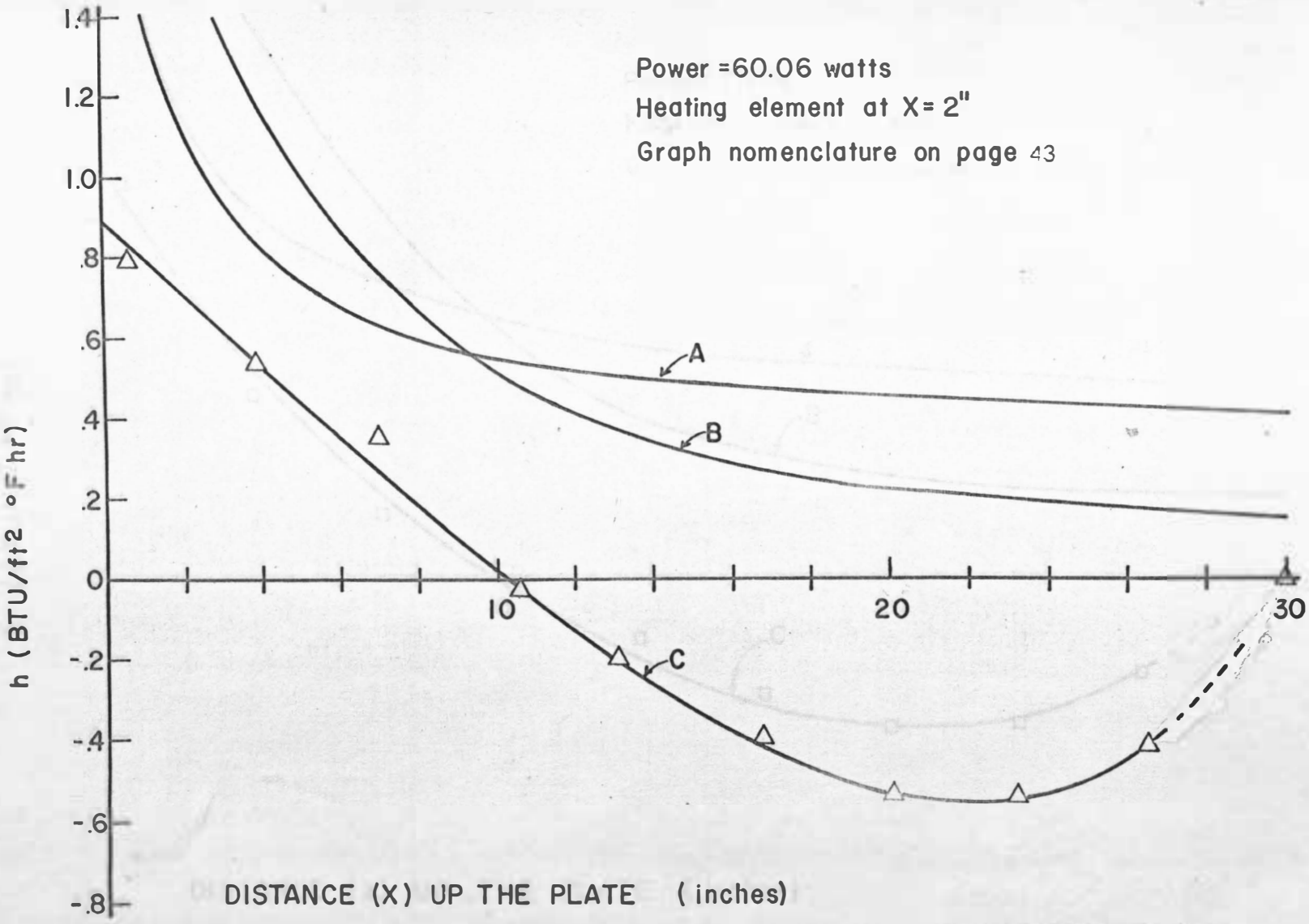

FIGURE 15 DISTRIBUTION OF HEAT TRANSFER COEFFICIENT (h)

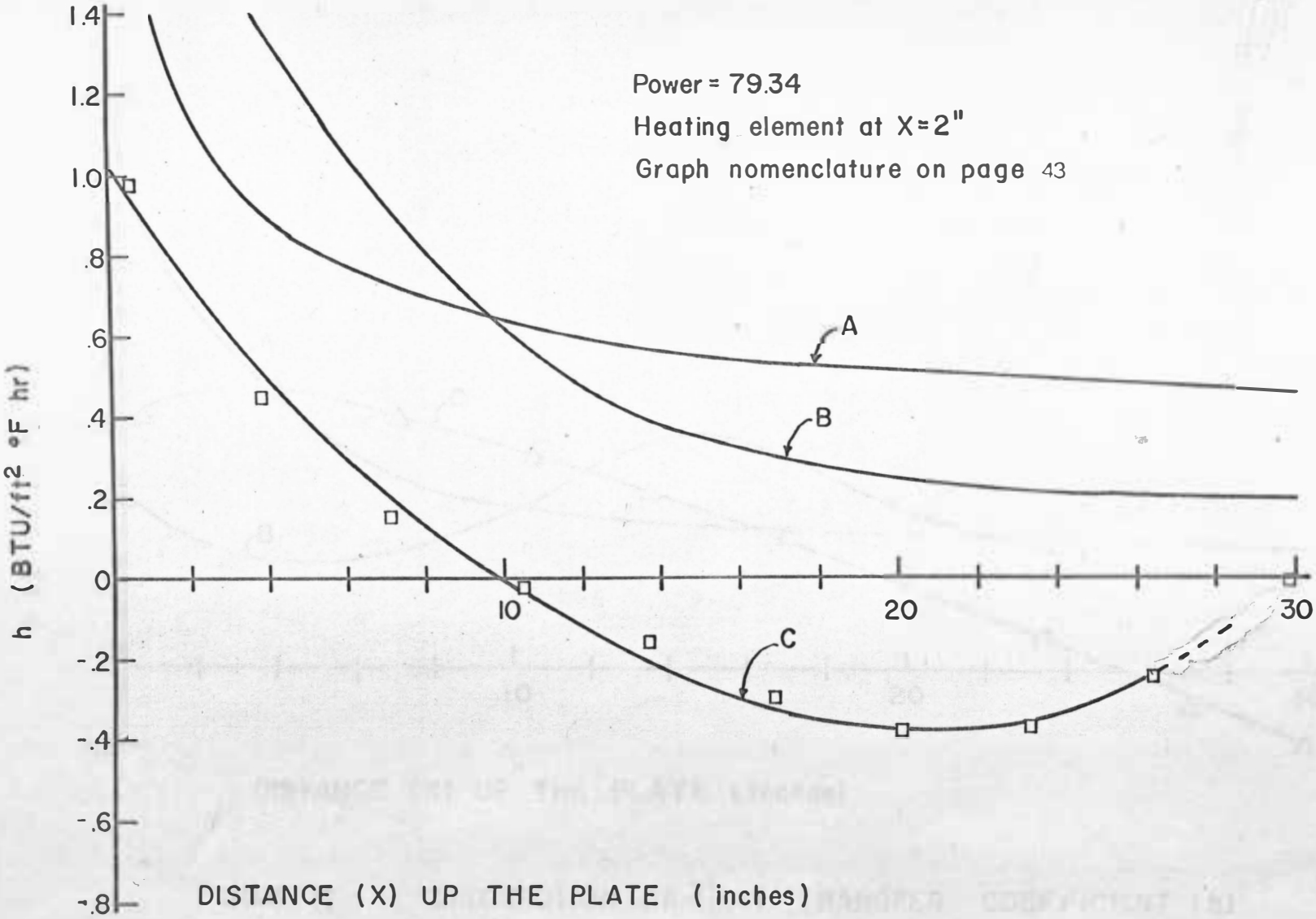

FIGURE 16 DISTRIBUTION OF HEAT TRANSFER COEFFICIENT (h)

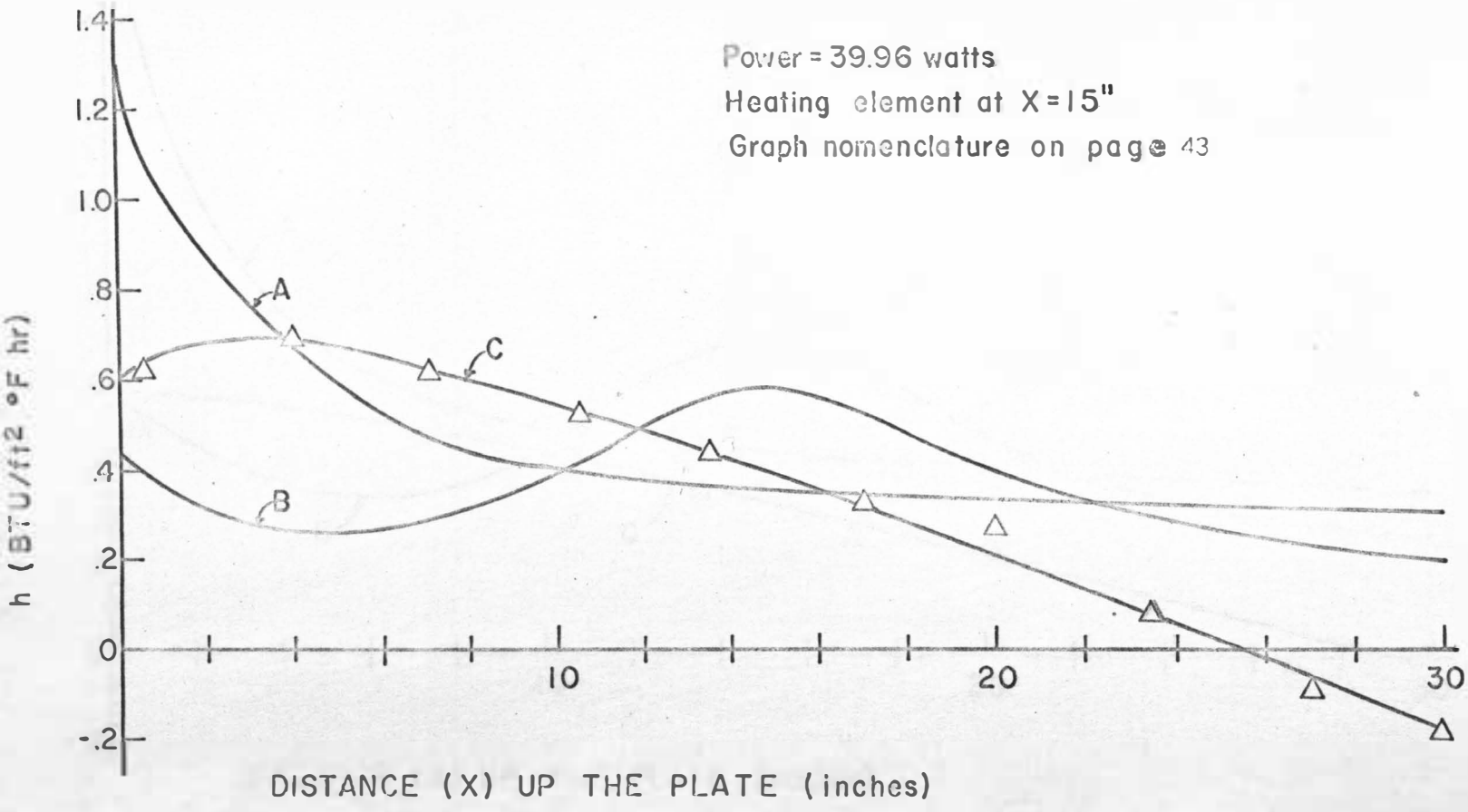

FIGURE 17 DISTRIBUTION OF HEAT TRANSFER COEFFICIENT (h)

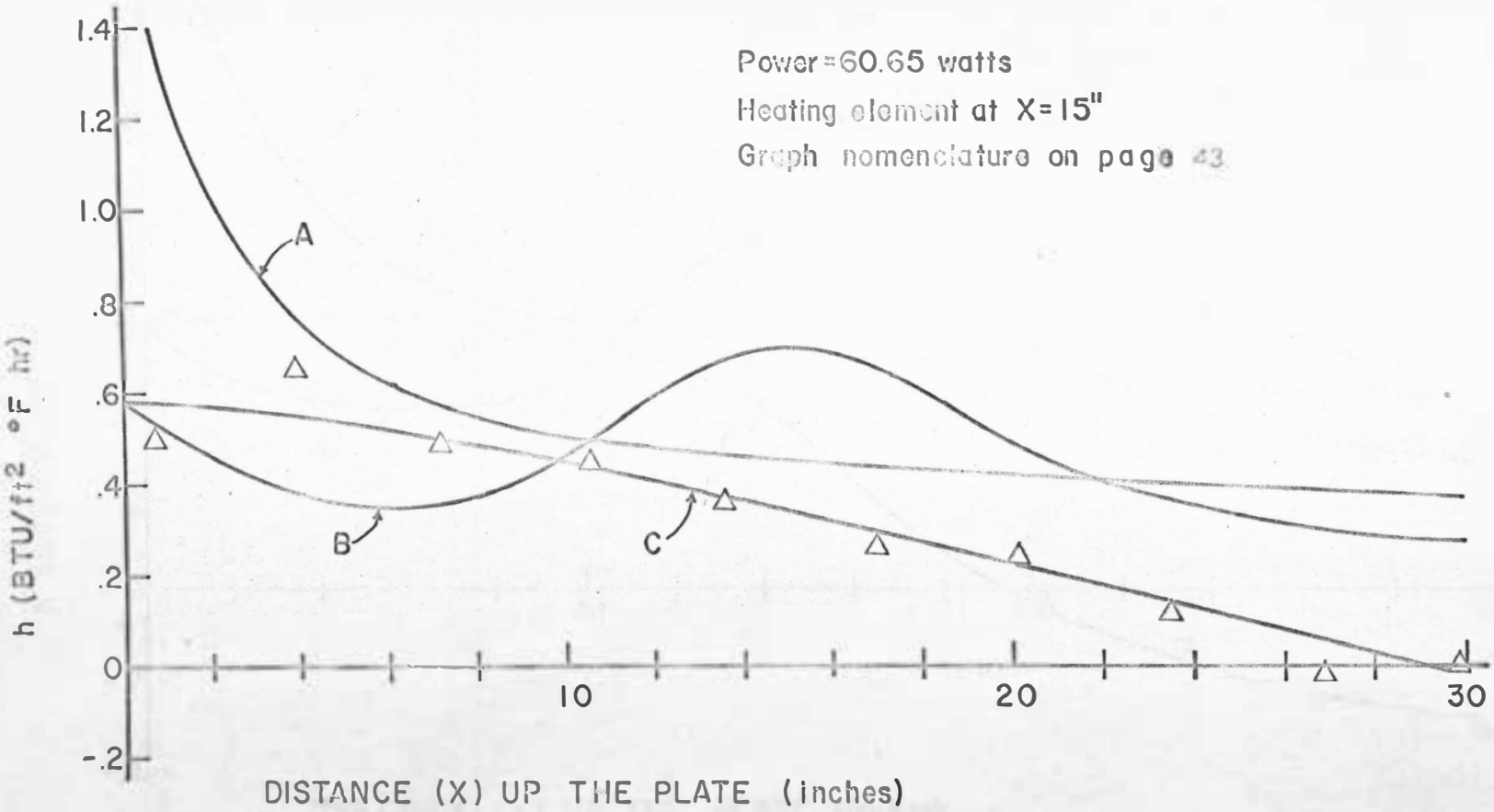

FIGURE 18 DISTRIBUTION OF HEAT TRANSFER COEFFICIENT (h)

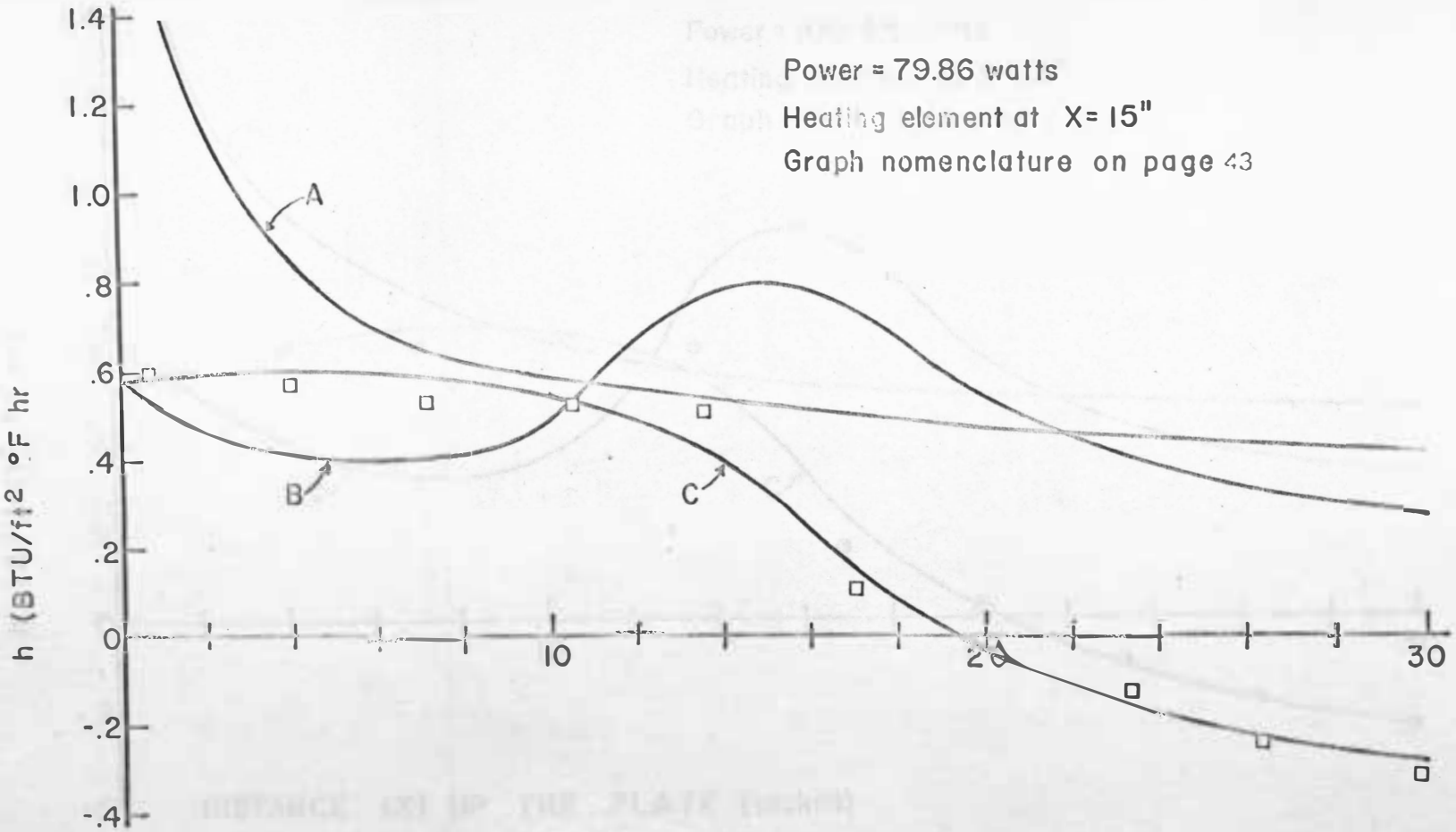

FIGURE 19 DISTRIBUTION OF HEAT TRANSFER COEFFICIENT (h)

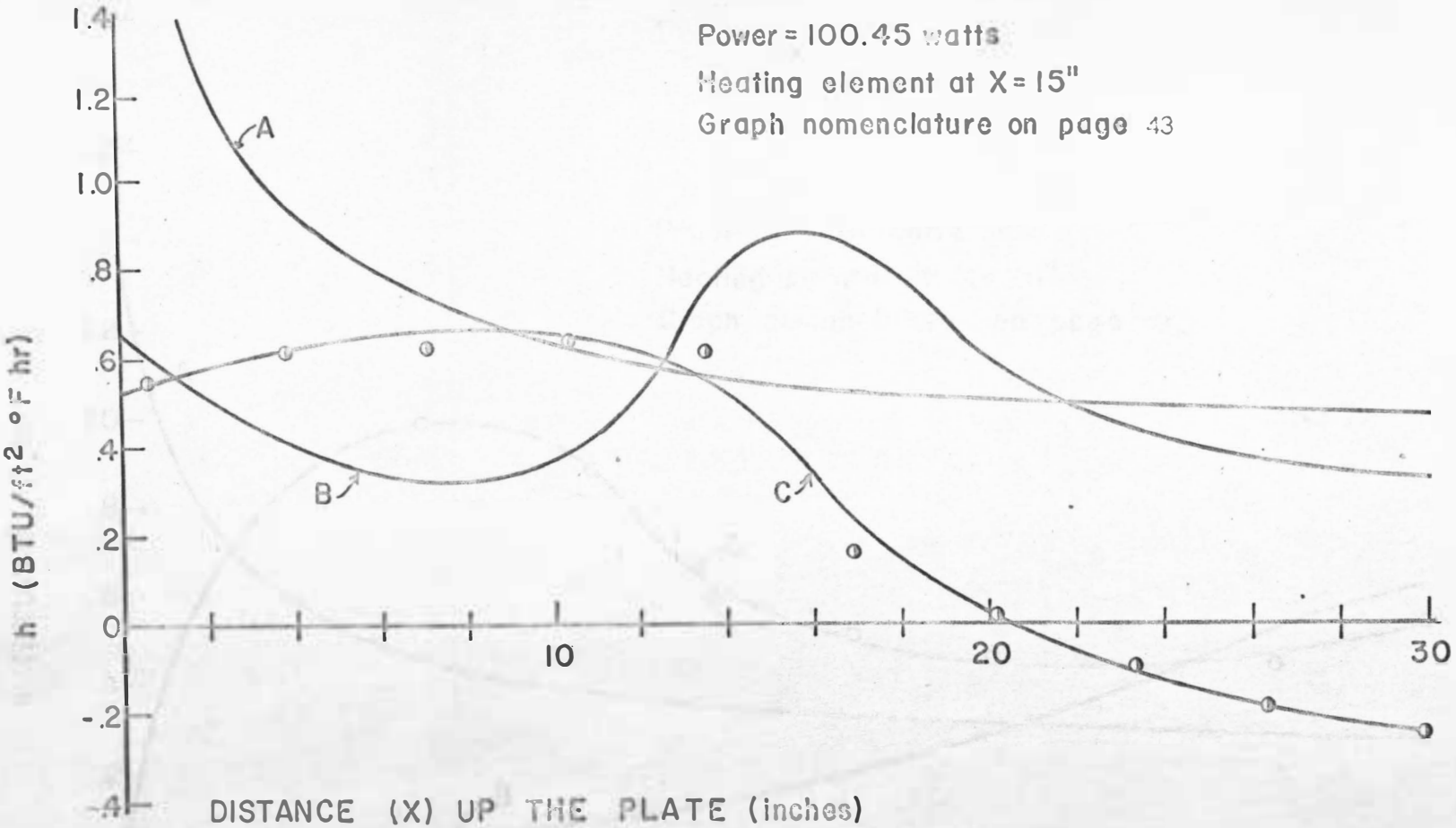

FIGURE 20 DISTRIBUTION OF HEAT TRANSFER COEFFICIENT (h)

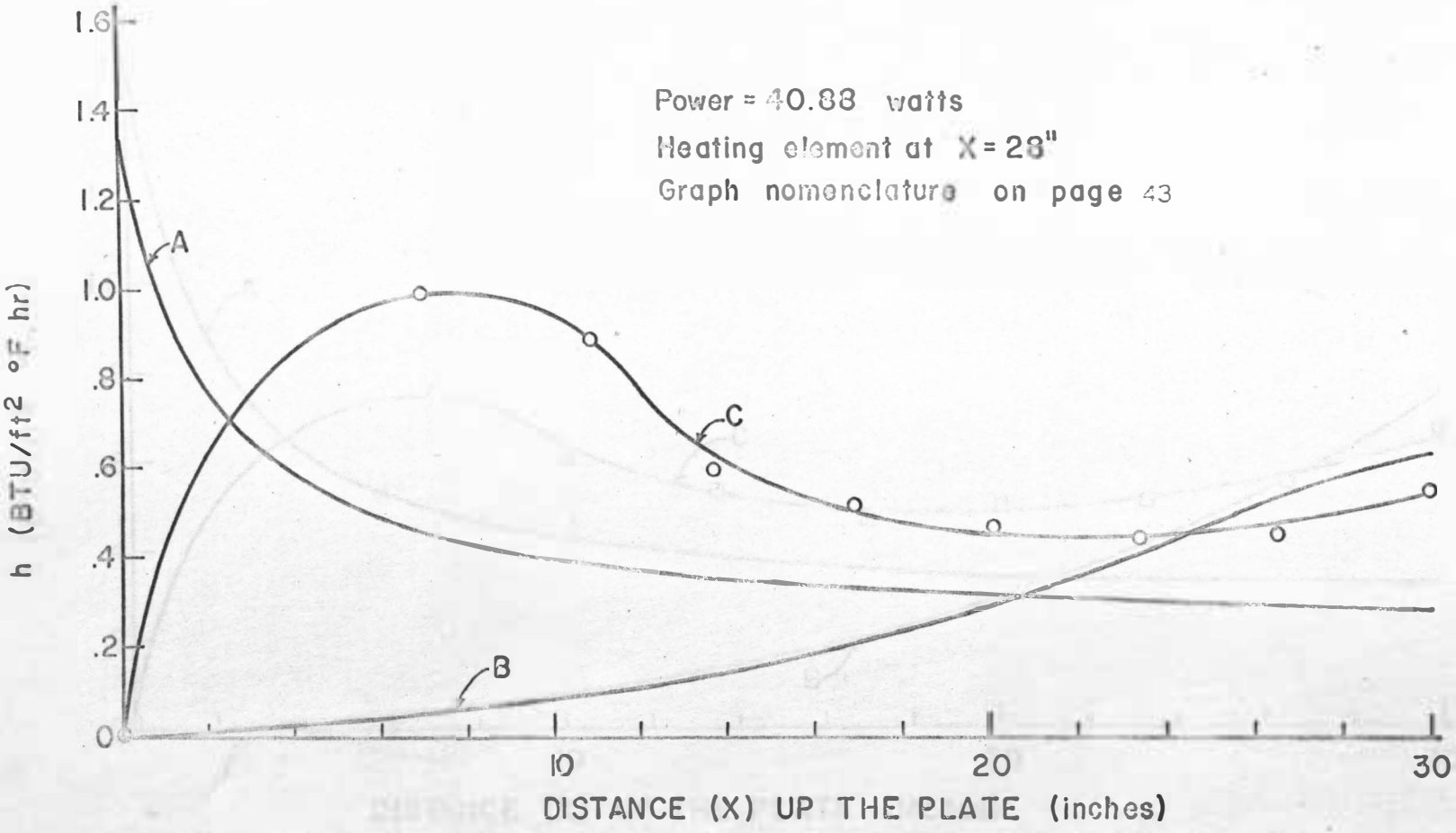

FIGURE 21 DISTRIBUTION OF HEAT TRANSFER COEFFICIENT (h)

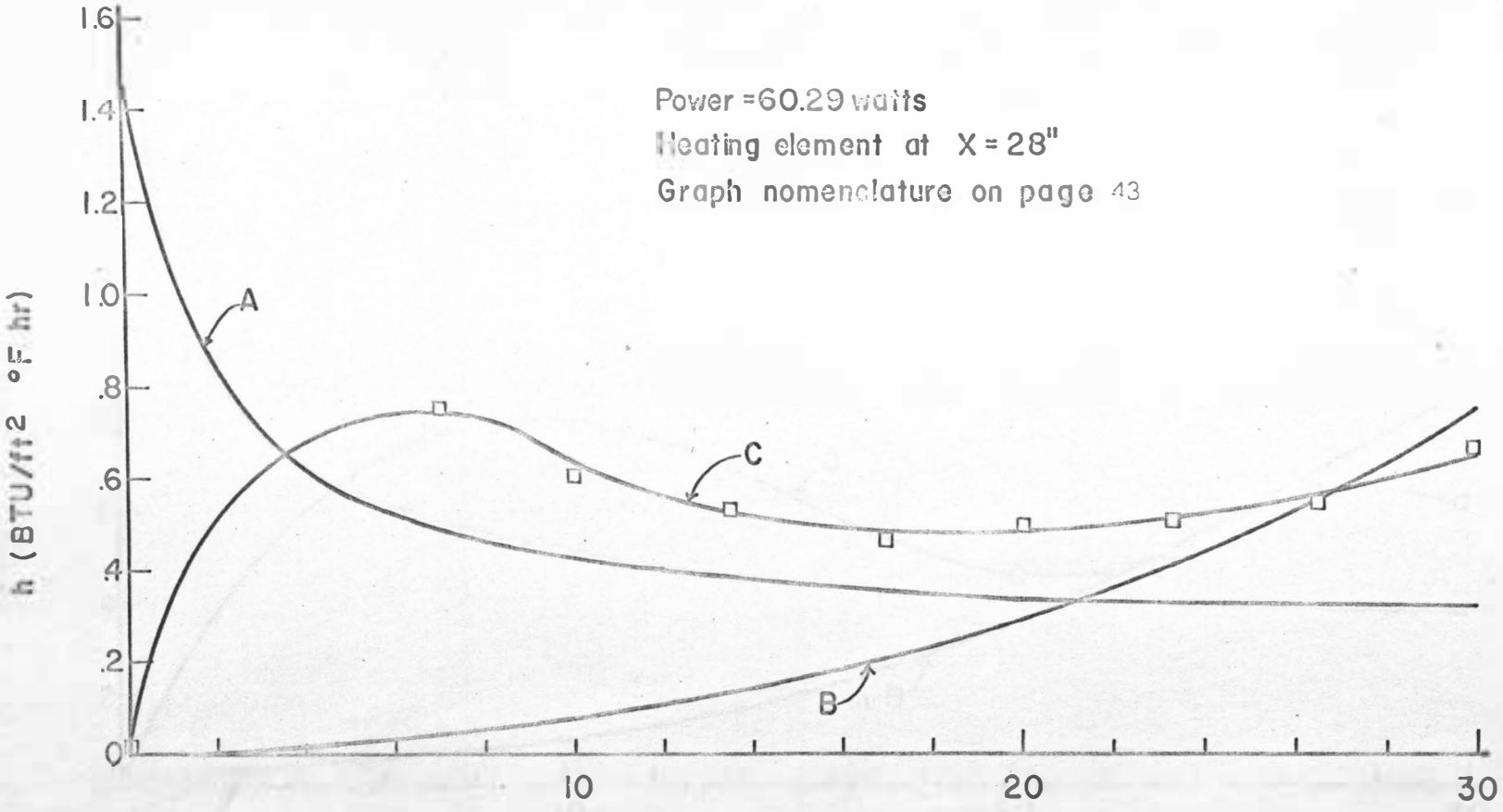

FIGURE 22 DISTRIBUTION OF HEAT TRANSFER COEFFICIENT (h)

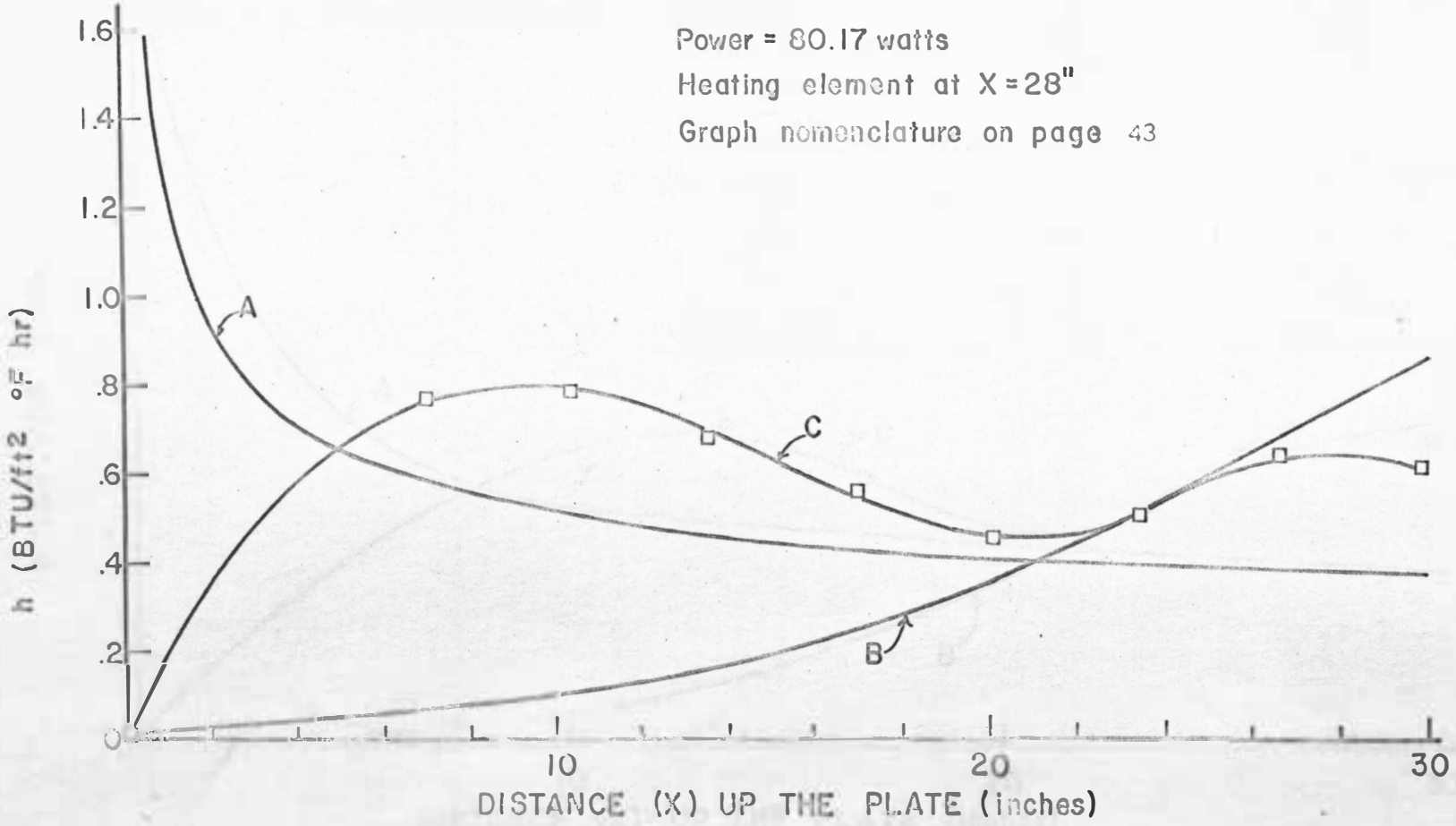

FIGURE 23 — DISTRIBUTION OF HEAT TRANSFER COEFFICIENT (h)

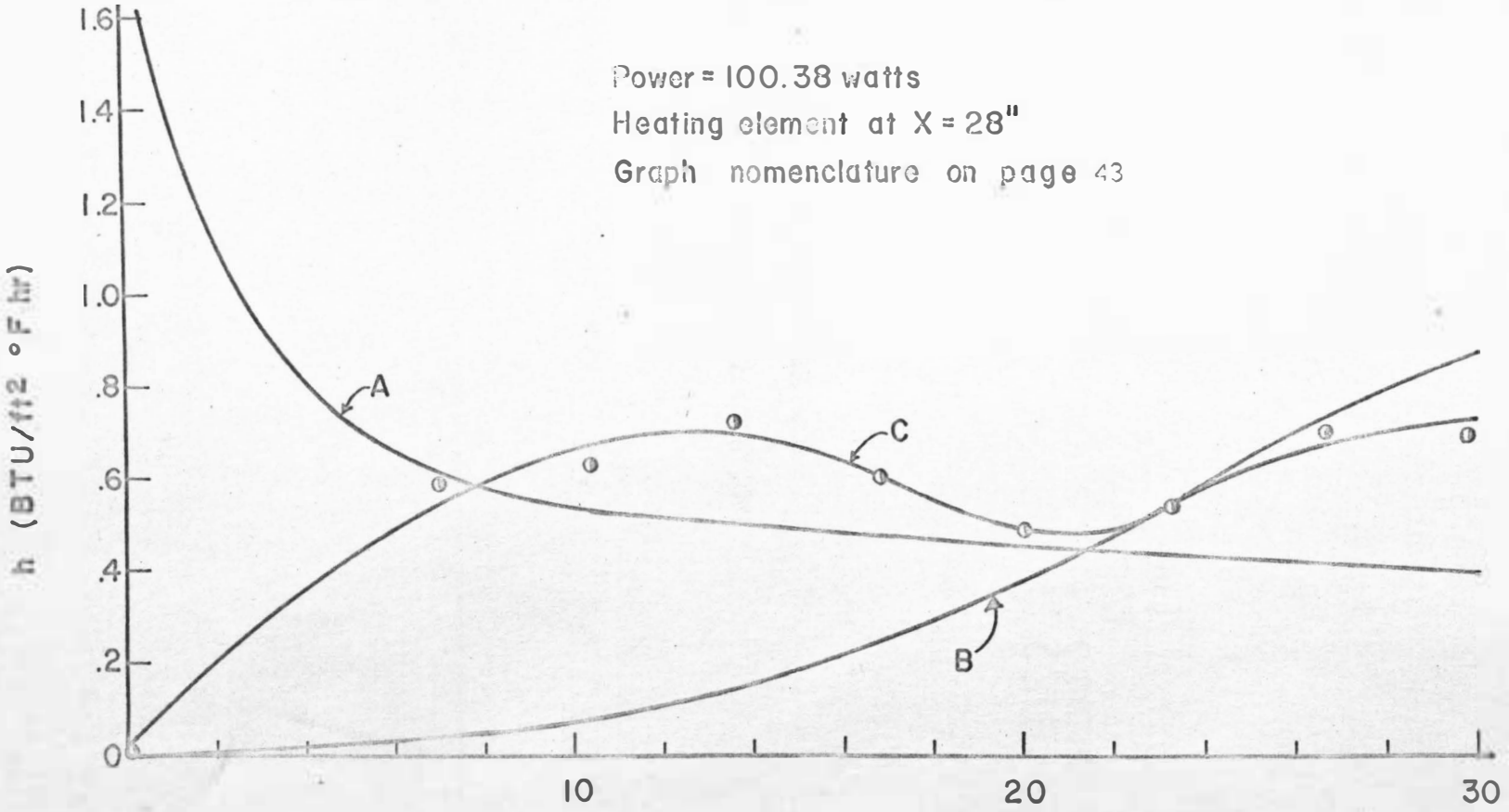

FIGURE 24 DISTRIBUTION OF HEAT TRANSFER COEFFICIENT (h)

APPENDIX B

SAMPLE CALCULATIONS

SAMPLE CALCULATIONS*

1. Calculation of Temperature (T_w)

$$\Delta T = \frac{\Delta N \times T_\omega}{\left(\frac{n-1}{\lambda}\right) \times b' - \Delta N}$$

T_ω = °R

$b' = b + 0.05\,b$ = mm.

$$\Delta T = \frac{24 \times 547}{\left(\frac{27.1 \times 10^{-5}}{63.3 \times 10^{-5}}\right) \times 183.9 - 24} = 248°$$

$$T_w = T_\omega + \Delta T$$

$$T_w = 87°F + 248°F = 335°F$$

T_w (measured) = 330°F

2. Calculation of Temperature Gradient

$$\frac{dT}{dy} = \frac{\Delta N/\Delta Y \times T_\omega}{\left(\frac{n-1}{\lambda}\right) \times b'}$$

T_ω = °R

ΔY = inches

$$\frac{dT}{dy} = \frac{(24/0.355) \times 800}{\left(\frac{27.1 \times 10^{-5}}{63.3 \times 10^{-5}}\right) \times 183.9} = 686\ °F/inch$$

* All calculations are made for a heating element position at x = 28 inches and a power setting of 100.38 watts.